UK UNLIMITED

ATOMIC WEAPONS ESTABLISHMENT

AWE REPORT No. O 20/90

The Detection and Location of Near-Regional Seismic Disturbances by the Eskdalemuir Array: A Study using Noise and Signal Correlations

R C Lilwall

Recommended for issue by

A Douglas, Superintendent

Approved by

B L Elphick, Head of Division

CONTENTS

SUMMARY

Recordings of noise and of signals from seismic disturbances at near regional (0 to 500 km) distances are used to investigate the noise and signal correlations for the Eskdalemuir array. At frequencies below 0.33 Hz the noise is dominated by microseisms which are highly coherent across the array and mainly have backbearings in the NW quadrant and slownesses around 0.28 s/km. At progressively higher frequencies the noise correlation declines, until above 2 Hz the noise is uncorrelated even for adjacent seismometers separated by 0.9 km along the array arms. Above 2 Hz any systematic negative noise correlation appears to be at most -0.05. Signal correlations are influenced by the length of the time window used in aligning the different channels since this frequently determines whether either or both Pg and Pn arrivals are present. In general correlations in the 2-8 Hz band based on time windows of 1-2 seconds following the P-wave onset are found to fall to 0.5 at seismometer separation distances corresponding to 2-3 horizontal wavelengths. The observed spatial variation of the signal and noise correlations enable predictions to be made on the beamforming capability of the array in terms of potential signal to noise gain. Predicted gains are 3.8 in the 2-4 Hz band falling to 3.0 in the 6-8 Hz band when using the full 20 seismometer array. The uniform spacing of the seismometers in the array leads to strong grating lobes in the array response which in turn can lead to ambiguities or aliasing in estimates of the slowness and backbearing of incoming signals. This problem is considerably reduced if only signals with slowness less than 0.2 s/km (apparent velocity in excess of 5 km/s) are considered. Standard errors on the backbearing estimates for near regional signals are found to be in the range 3 to 4°.

1. INTRODUCTION

The Eskdalemuir Seismometer Array (EKA) in Dumfriesshire, Scotland began recording in 1963 and has maintained near continuous operations until the present time. The array has provided much data for research undertaken by the MOD seismological group at Blacknest and also by other workers both in the UK and abroad. In recent years EKA has been the UK station used to provide data in support of the Ad Hoc Group of Scientific Experts (AHGSE) activities in Geneva.

Although improvements have been made over the years in the mode of recording and processing the data at EKA, the array (figure 1) has remained essentially unchanged since installation. The array geometry, 20 seismometers with fixed 0.9 km spacing in a simple linear cross, was determined partly by the analogue equipment available in the early 1960's (ie 23 channel tape recorders and fixed delay options between channels during processing). The design was also influenced by a seismological objective considered important at the time; the detection of 1-2 Hz P_n signals from explosions at regional distances of up to 1000 km. The relatively low frequencies of these signals reflect early observations at such distances from the Nevada Test Site (NTS) and together with the 8 km/s horizontal wave speed for P_n, resulted in the use of a 9 km arm length for EKA and a similar experimental array at Pole Mountain, Wyoming, USA. Early observations from these arrays however, lead to a switch in interest from observing regional signals to the much higher wave speed arrivals at teleseismic distances. Arrays for recording at teleseismic distances were then installed at

Yellowknife (YKA), Canada, Warramunga (WRA), Australia and Gauribidanur (GBA), India and have twice the aperture of EKA. For all these arrays the aperture was chosen to be approximately the horizontal wavelength of the signals of interest.

In recent years there has been revival of interest in the use of arrays for the detection and location of seismic disturbances at regional distances. The relatively efficient propagation of crustal and sub-crustal seismic phases over much of northern Europe and north west USSR means that the best signal-to-noise ratio (S/N) for the arrivals tends to be at higher frequencies than found for NTS explosions. In addition the possibility of decoupling nuclear explosions means that monitoring compliance with a future comprehensive test ban or low yield threshold treaty will involve the use of signals detectable only at regional distances. As a result arrays such as NORESS in Norway, which have been designed to exploit the observed signal and noise properties at higher frequencies, are much smaller in aperture than EKA. Although the potential of EKA for investigating seismic events within the UK region was revealed in some early work, (eg, Key, Marshall and McDowell (1), Cleary (2)), most use has been made of data from seismic disturbances at teleseismic distances. At present (1990) routine beamforming and detection at EKA are only made for teleseismic signals and continuous digital recording is made at 20 samples per second with no provision for the aliasing problem introduced by high frequency (>10 Hz) signals. Data for such signals must be obtained via analogue recordings.

The work described in this report was prompted by the increased interest in recordings at regional distances and also by the imminent cessation of analogue recording with possible future enhancement of the digital recordings to include higher frequencies at EKA. In particular it is desirable to know the "high" frequency capabilities of the current or alternative array geometries at the present location in terms of the enhancement of the S/N ratio of the signals of interest by beamforming and also in the ability of the array to locate the source of the signals. Many properties of an array can be described with the use of the theoretical array response as described by Birtill and Whiteway (3) but conclusions are dependent on assumptions about both noise and signal properties. In this report the array capabilities are investigated using the observed spatial noise and signal properties across the array and is similar to techniques described by Mykkeltveit et al (4) in their study of the NORESS site. The data used are taken from the routine analogue and digital recordings at EKA. Limitations in the analogue recording system mean that the highest frequency considered is 8 Hz, which although high for teleseismic recordings is low when considering arrivals from sources such as local quarry blasts. Nevertheless optimum S/N ratio for all but the nearest sources usually occurs below 10 Hz and hence such data have an important role in seismic detection.

2. NOISE AND SIGNAL PROPERTIES AT EKA

The success of beamforming in enhancing the S/N ratio depends on the properties of the incoming wavefield. The signal should have an approximately plane wavefront so that the recorded outputs from the seismometers (henceforth referred to as the array channels) can be easily aligned to allow for the propagation delays across the array. Furthermore, the signals should be well correlated in the frequency band of interest. Finally the background noise should have zero or negative correlation. These requirements are reflected in the following equations which give the S/N amplitude gain G, obtained with beamforming with an N sensor array:

$$G^2 = \frac{\sum_{j=1}^{N} \sum_{i=1}^{N} c_{ij}}{\sum_{j=1}^{N} \sum_{i=1}^{N} \rho_{ij}} \qquad (1)$$

where c_{ij} and ρ_{ij} are the inter-channel correlations of the signal and noise respectively between channels i and j after allowing for the propagation delays of the signal. The correlation between channels i and j is defined as:

$$c_{ij} \text{ or } \rho_{ij} = \frac{\sum_{k=1}^{M} s_i(k)s_j(k+t_j)}{(\sum_{k=1}^{M} s_i(k)^2 \sum_{k=1}^{M} s_i(k+t_j)^2)^{0.5}} \qquad (2)$$

where $s_i(k)$ is the kth signal or noise sample from channel i, t_j is the time delay in samples required for alignment for channel j, M is the length in samples of the time window used. If the signal waveforms are all perfectly correlated (all $c_{ij} = 1.0$) and the noise uncorrelated ($\rho_{ij} = 0.0$ $i \neq j$; $\rho_{ij} = 1.0$ $i=j$) then the S/N gain given by equation (1) reduces to $\sqrt{N}$, a value frequently assumed. The gain will be less than this if the signals are less than perfectly correlated or the noise is positively correlated. On the other hand gains greater than $\sqrt{N}$ are possible if there are negative correlations in the noise.

Clearly knowledge of the spatial properties of both noise and signals through the inter-channel correlations c_{ij} and ρ_{ij} is of great value in assessing the capability of an array as was found by Mykkeltveit et al (4) in designing the configuration of NORESS. The next section therefore describes an investigation of the quantities c_{ij} and ρ_{ij} for EKA.

2.1 Noise properties

Noise samples taken from digital recordings during 1989 were used to study noise properties at EKA. To allow for possible diurnal and seasonal variations the samples were

taken at 0300, 0900, 1500 and 2100 hours GMT on one day for each month. Directly recorded digital rather than digitised analogue data were used because the latter are found to be degraded by system noise especially from incomplete flutter compensation on the analogue playback. Such system noise was found to have zero delays between channels with correlations of up to 0.15 between channels.

2.1.1 Noise power spectra

Although the main interest in this report is the spatial noise properties at EKA, for completeness, the noise amplitudes are described in this section. Noise power spectra were computed using 50 s cosine tapered (10%) time windows for each sample. The windows were chosen to avoid:

(i) interference and glitches clearly of non-seismic origin;

(ii) seismic event arrivals; and

(iii) noise bursts of short duration presumably due to cultural activity near the array.

The latter two were most common in the samples at 1500 h because of quarrying and other human activities. Power spectra were computed for each of the 20 channels, stacked, and the result smoothed. The stacked spectra are taken as representative of the array. These spectra were then grouped by time of day and a further stacking performed. The process was repeated with the spectra grouped by season. Figures 2 and 3 show the final stacked noise spectra for time of day and season respectively.

The diurnal variation shown in figure 2 shows that all the spectra are similar except that the samples taken at 1500 h are slightly more noisy than the rest (+5 dB) at the higher frequencies. As expected the seasonal variation shown in figure 3 indicates higher noise levels during the winter months than during the summer. Noise levels are 10 dB up at 0.3 Hz from October to March and 5 dB up at 8 Hz from January to March, when compared with April to September. Figure 4 shows the overall stacked spectrum for all 48 samples together with those for "quiet" and "noisy" days published in Bache, Marshall and Young (5). All three spectra converge at the higher frequencies but in the lower frequency range the average found in this study is similar to the "noisy" day example. This is not surprising since quiet days characterised by calm sea conditions in the N Atlantic are rare, and it will be seen in the next section that most samples taken in this study have spatial noise characteristics corresponding to microseisms propagating from the north west, presumably because the nearest area of rough sea lies in that direction.

2.1.2 Noise correlations

S/N ratio gains obtained by array beamforming depend on the noise being zero or negatively correlated between channels, after allowing for the propagation delays of the signal. The noise properties were investigated by computing the correlations between the noise recorded on each channel pair of the array for each of the noise samples as described above (equation 2). Channel delays t_j were used which correspond to plane wavefronts defined by a range of slowness vectors S (S being defined by slowness and backbearing). To enable the insertion of delays with sufficient accuracy for the higher frequencies the fast Fourier transform was used to interpolate between samples and so increase the sampling rate from 20 to 80 samples per second but leaving the spectra unchanged. Altogether 119 slowness

vectors S were used corresponding to backbearings well distributed around the array, and slowness from 0.0 to 0.4 s/km (horizontal wave speeds from ∞ to 2.5 km/s).

The mean correlation $\hat{\rho}$ of all the seismometer pairs for each of the noise samples was computed for each S. Here and elsewhere in the report mean correlation ($\hat{\rho}$) is computed by first applying Fishers z transform ($z = 0.5\ \mathrm{Log}_e((1+\rho)/(1-\rho))$) to the individual values, finding the mean $\hat{z}$ and then finding the inverse transform $\hat{\rho} = \tanh(\hat{z})$. This procedure avoids the bias introduced if the original correlations are simply averaged.

Figure 5 shows the mean correlation for all 48 samples contoured as a function of S using frequency bands 0.125-0.25, 0.20-0.33 and 0.33-1.0 Hz. Similar plots for higher frequency bands all have overall means below 0.05 (the minimum contour value). Microseismic noise originating from the N Atlantic is the main noise source at low frequencies, the dominant value for S (slowness 0.28 s/km; backbearing 315°) being similar to that found by Douglas and Young (6) for microseisms observed in Southern England. It is not possible to determine with this data if the more isotropic distribution seen in figure 5 for the 0.33-1.0 Hz band results from scattering or from an additional noise source in the North Sea. Figure 5 shows positive average noise correlations at frequencies less than 1 Hz for most slowness vectors S, hence even if an incoming signal is well correlated equation 1 predicts S/N gains less than $\sqrt{N}$ when beamforming. At higher frequencies the average noise correlations of near zero (not plotted) show that $\sqrt{N}$ gain could be achieved provided the signals are well correlated.

In figure 6 the nature of the noise is shown in terms of the location of the slowness vector S giving the maximum mean correlation $\hat{\rho}$ for each of the 48 noise samples. The size of each symbol is proportional to the mean correlation. The mean slowness increases slightly from 0.273 ± 0.005 s/km for the 0.13-0.25 Hz band to 0.291 ± 0.007 s/km in the 0.33-1 Hz band. At frequencies above 1 Hz figure 6 shows that average correlations are near zero.

To establish whether alternative array geometries can be used to exploit the noise properties it is useful to know how the noise correlation ρ_{ij} changes with seismometer separation D_{ij}. Figures 7 to 9 show this variation for the 2-4, 1-2 and 0.33-1.0 Hz frequency bands respectively. To produce these figures the correlations between each channel pair for fixed slowness are first averaged over all the 48 noise samples and all backbearings. These means are then grouped and averaged in 0.1 km distance cells for seismometer separation D. Figure 7 shows that at frequencies above 2 Hz the noise is uncorrelated at distances greater than 0.9 km, the seismometer separation along the array arms. Measured correlations at distances less than about 0.9 km all include data from channel B4 near the array arm crossover. At these small separations and at slownesses corresponding to most P arrivals (0.0-0.166 s/km) the correlations appear to show a small negative swing before presumably rising to unity below 0.4 km distance. This feature is poorly resolved because of lack of measurements at short distances but its amplitude is less than 0.05 and is therefore smaller than that found by Mykkeltveit et al (4) for the NORESS array site. At frequencies below 1 Hz the noise is positively correlated at seismometer separations less than 1-3 km (figures 8 and 9). The reduction in S/N gain with beamforming resulting from these positive correlations is compensated for to some extent however by the presence of negative correlations at greater separations.

2.2 Signal properties

2.2.1 Signal data used

Signal correlations across the array were investigated using recordings of P arrivals from a selection of near-regional seismic disturbances (mostly 40-500 km epicentral distance). The data were chosen on the basis of having a good S/N ratio (greater than 4/1) and from seismic sources that are well distributed around the array.

Aliasing makes the routinely recorded 20 samples/s digital data unsuitable to study many of the relatively high-frequency signals from seismic disturbances at these distances. Instead, but at the expense of introducing system noise, data digitised at 40 samples/s from analogue recordings were used. In practice limitations in the dynamic range of the existing analogue recording system means that recordings of signals which would have high S/N over the whole frequency range studied here (2-8 Hz) are clipped and so cannot be used. Peak S/N ratios are limited to the range between about 4:1 to 30:1. Altogether recordings of signals from 58 seismic sources were used most of which are believed to be natural but a few are known quarry blasts. The distribution of these sources about the array is shown in figure 10. To enable accurate computation of the correlations for frequencies up to 8 Hz the sampling rate was increased from 40 to 160 samples/s using the same technique employed with the noise data.

2.2.2 Computation of signal correlations

Using the data described above the signal correlations c_{ij} between each of the seismometer pairs were calculated using the equation 2. The time lags t_j required to align the channels were calculated from the signal slowness vector. Deviations from a plane wavefront become significant in this study for epicentral distances less than about 100 km. To enable signals from sources at such short distances to be studied, the time lags were calculated assuming the wavefront is a circle centred on the source, and hence an approximate distance to each source was required.

Two criteria were tried to determine the slowness vector for each signal. The first finds the slowness vector *S* which maximises the mean inter-channel correlation $\hat{c}$ using a short time window starting at the P onset. The mean $\hat{c}$ is defined in the same way as $\hat{\rho}$ in section 2.1.2. The second criterion maximises the mean power of the array sum for a similar window. For both methods the time series were first 2-8 Hz bandpass filtered since at higher and lower frequencies the S/N ratio is generally poor. The slowness vectors were obtained by searching through a course grid of 400 values (spacing 0.02 s/km) to get the approximate maximum and then repeating using progressively finer slowness vector grids. These slowness vector determinations were repeated using time window lengths of 0.5, 1.0, 1.5 and 2.0 s starting at the P onset.

A problem arises from the presence of grating lobes in the array response which often result in convergence on false maxima for the slowness range 0.00-0.33 s/km, designed to cover likely P and S arrivals. This is illustrated in figure 11 which shows the estimated slowness values plotted as a function of epicentral distance. Many of the maxima are at spuriously high slownesses for crustal P waves, especially when a 0.5 s time window is used. The presence of grating lobes is exaggerated because many of the waveforms have low amplitude initial onsets followed quickly by arrivals with larger amplitude and often different slowness. The form of these seismograms is the result of the superposition or overlap of P_g

and P_n type phases and means that routine determination of slowness and back-bearing using the present EKA array geometry must be done with caution. The problem is reduced slightly when optimising correlation rather than average power and since only P phases are being considered it can be resolved by reducing the slowness range to that of crustal P waves, ie 0.0-0.2 s/km. The resulting slowness values, plotted in figure 12, clearly show a gradual change with increasing epicentral distance, from purely crustal P_g arrivals (slowness = 0.166 s/km; speed = 6 km/s) to upper mantle P_n arrivals (slowness = 0.125 s/km; speed = 8 km/s). The results appear stable for window lengths of 1.0 s and above.

These observations suggest that the inter-channel correlations are best studied using channel alignments based on slowness vectors optimised for mean coherence and 1-2 s window lengths. Windows of 1 and 2 s were therefore used to determine the optimum beam and the resultant correlations were computed using the 2-8 Hz bandpass and also narrower bands of 2-4, 4-6 and 6-8 Hz.

2.2.3 Mean inter-channel correlations

Figure 13 shows the mean inter-channel correlation $\hat{c}$ calculated for four window lengths using three frequency bands and plotted as a function of epicentral distance. Channel alignments correspond to beams optimised using a 2 s time window with the result that mean correlations are highest for the longer (1.5 and 2.0 s) windows. The pattern of correlations is changed in figure 14 where a 1 s window is used to determine the beams used for channel alignment. Predictably the correlations are now highest for the 1 s window. Greater scatter in the mean correlations for sources at epicentral distances between about 90-250 km compared with other distances is present in both figures 13 and 14. This probably results from the superposition of arrivals such as Pn and Pg with more than one distinct slowness within the window.

Both figures 13 and 14 show that overall mean correlations decline with increasing signal frequency. In the 2-4 Hz band mean correlations are in excess of 0.5 and, assuming the noise is incoherent, S/N gains approaching $\sqrt{N}$ should be obtained if the full array is used for beamforming. For the 6-8 Hz band mean correlations are almost half those in the 2-4 Hz band and hence the potential S/N gain is reduced.

2.2.4 Variation of correlation with seismometer separation

To study the effect of using alternative array geometries on the beamforming gain, it is necessary to know the variation of the inter-channel correlations c_{ij} with the spatial separation of the seismometers D_{ij} rather than their mean $\hat{c}$ for the existing geometry. A sample of plots showing this variation for selected events are illustrated in figure 15. These mostly show the correlations falling with increasing separation but with considerable scatter. Systematic variation from a regular decline of correlation with separation may result from uneven sampling in space because of the relation of the array arms with respect to each incoming wavefront. To define the underlying variation of correlation with separation distance, the results for all the seismic sources were averaged. Since the scatter in the mean correlations appears to change with epicentral distance Δ, the data were grouped into three distance ranges; Δ <90 km, 90<Δ<250 km and Δ>250 km. Correlations c_{ij} computed for all the seismic events in each range were grouped in 0.5 km cells in separation D_{ij}. Figure 16 shows the resulting cell means for the 2-8, 2-4, 4-6 and 6-8 Hz frequency bands for correlations based on a 2 s alignment window. Figures 17 show the equivalent results obtained using a 1 s window. The curves plotted in both figures are fitted to the cell means

by least squares and have the exponential decay:

$$C = ae^{-(D/d)} \qquad (3)$$

where C is the cell mean correlation at separation D km, d and a are constants with a set to unity for the solid curves. Clearly the simple exponential decay (a set to unity) is only a rough fit to the observed values which often fall systematically below and above the solid curve at small and large separations respectively. Better fits, shown by the dashed curves, are obtained by letting the constant a in equation (3) vary, but this is difficult to justify on physical grounds because at short distances the true correlations must always tend to unity. The presence of noise in the recordings may account for some of the observed deviations and in particular the reduced correlation at short separations. In addition incorrect alignment of the channels will result in a decrease in correlation.

Figures 16 and 17 show that in general the fall-off in correlation with separation distance as quantified by d is 2 to 3 times more rapid in the 6-8 Hz band than in the 2-4 Hz band. This suggests that the characteristic distance d in equation (3) could be expressed in terms of a number of wavelengths and the equation generalised to:

$$C = ae^{-(D/n\lambda)} \qquad (4)$$

with λ the wavelength and n a (non integer) constant. Assuming an average wave speed of 7 km/s, for P waves in the material under the array, the average wavelengths λ are 2.33, 1.40 and 1.0 km for the 2-4, 4-6, and 6-8 Hz bands respectively. Combining the data from all three epicentral distance ranges, the average number of wavelengths n represented by the value of d is 4.1 ± 0.2 for the 2 s window (figure 16) and 6.6 ± 0.6 for the 1 s window (figure 17). The constants d and n correspond to a fall in correlation to 0.37 (ie, 1/e). Lower falls such as to 0.5 or 0.6 are sometimes used to define these constants and the values of d and n obtained here are then approximately halved. These still represent several wavelengths however and, if source-receiver reciprocity can be assumed, the fall in correlation is much slower than those observed by Geller and Muller (7) on signals from adjacent sources. Their observations lead Geller and Muller to propose the hypothesis that correlations fall to 0.5 when sources are separated by only one quarter of a wavelength. It is worth noting that studies which apparently support this hypothesis use relatively long time segments to compute the correlations whilst this study and also that of Thorbjarnardottir and Pechmann (8), use shorter time segments and find much longer correlation distances.

2.2.5 Delay corrections

Deviations from the wavefront geometry assumed in aligning the array channels will tend to reduce the measured correlations. These deviations arise from velocity inhomogeneity which distorts the wavefront as the rays diverge along the path between source and individual seismometers. Large scale inhomogeneity, tends to distort the whole wavefront in a systematic way and is "absorbed" by a shift in the measured slowness vector leaving the channels well aligned. More random perturbations affecting individual channels however result in misalignment and reduced correlation. A simple way of removing this is to allow additional time shifts between each of the channel pairs to maximise the correlation. Artificially high correlations will be obtained however if the time windows are short and the data strongly band limited. This would occur in this study since the windows represent only a few cycles and therefore a compromise procedure was used to investigate the effect of allowing additional time shifts.

The channels were first aligned using the standard procedure assuming incoming circular wavefronts. The array sum was then formed and each individual channel cross-correlated against the summed time series for a range of additional time lags. Using the new time lags corresponding to the maximum cross correlations a new array sum was formed and the procedure repeated. A relatively broad 2-8 Hz band filter was first applied to the data.

Figure 18 compares the individual correlations with and without these additional shifts for the same selection of seismic sources used in figure 14. An improvement is visible in the correlations but it varies considerably from source to source. The correlation distance plots are compared in figure 19. The constants a and d are increased. Histograms showing the frequency distributions of the additional time delays are shown in figure 20 along with their mean and median values. Although some of the distribution means are significantly different from zero, they are all less than one sample at the original sampling rate of 40 Hz. One explanation of the delays is the effect of topography within the array. The heights of individual seismometers span almost 0.2 km and the associated topographic corrections have a similar amplitude to the observed mean delays. However it is clear in figure 21 that there is little correlation between time delays and topography. The delays may result from several other effects in addition to topography. These effects may be real, such as variation in superficial or deeper layer seismic wave speeds and some may be artifacts, such as differences in the recording and playback responses of the individual channels. Close examination of recorded waveforms and their spectra suggests that many of the data from sites R3 and B3 are probably distorted by deviations in the system response from the average.

3. BEAMFORMING GAIN FOR NEAR REGIONAL SOURCES

The expected beamforming gain can be calculated using equation 1 and the the estimated noise and signal correlations ρ_{ij} and c_{ij}. At frequencies above 2 Hz the noise is essentially uncorrelated between channels and hence the denominator of equation (1) is N. The empirical exponential fits defined by the constants a and d in figures 16 and 17 can be used to estimate the observed signal correlations c_{ij}.

Figure 22 shows the predicted S/N gains in the 2-4, 4-6 and 6-8 Hz bands using the correlations found for 2 s windows. The gains are the average calculated for the sets of array channels operating for each of the 58 seismic disturbances studied (average number of operating channels was 17.1). Also shown are the average observed S/N gains obtained by comparing the average spectral amplitudes in the 2 s windows for the individual channels with the spectral amplitudes for the array beam. The agreement between observed and predicted is generally good and gives confidence that equation (1) can be used to obtain good predictions of S/N gain for alternative array configurations.

The variation in the predicted gain for the three different epicentral distance ranges studied is small (figure 22) and therefore to summarise the results, the mean gains have been calculated. For the full 20 channels the gains in absolute terms and as a percentage of $\sqrt{N}$ are 3.83 (86%$\sqrt{N}$), 3.53 (79%$\sqrt{N}$) and 2.98 (66%$\sqrt{N}$) respectively for the 2-4, 4-6 and 6-8 Hz bands. The gain possible for the full array falls considerably as the frequency increases and is always less than $\sqrt{N}$. The performance of arrays consisting of subsets of the full array can be assessed by progressively removing the outer seismometers. The reduction in N tends to reduce the gain possible but this is partly compensated for by the increased correlations at the shorter distances involved. For configurations consisting of the inner 10 and 6 seismometers the gains are 2.87 (91%$\sqrt{N}$), 2.74 (87%$\sqrt{N}$), 2.51 (80%$\sqrt{N}$) and 2.27 (93%$\sqrt{}$), 2.20 (90%$\sqrt{N}$), 2.14 (87%$\sqrt{N}$) respectively. Although the potential gains are reduced they are more uniform over the frequency ranges.

4. COMPARISON OF BACK BEARING ESTIMATES

The determination of the slowness vector of the incoming wavefront enables the source epicentre to be estimated through separate estimates of epicentral distance and backbearing. It is clear from figure 12 however that the slowness can give only a rough estimate of the epicentral distance for sources in the 0-1000 km distance range. For this reason epicentral distance is usually estimated from time differences of phase pairs such as S-P even if the measured slowness is available. Neglecting the effect of lateral heterogeneity, backbearing estimates are independent of the variation in P-wave speed with depth on the path between source and array and provide an important constraint on the epicentre. It is therefore useful to quantify the capabilities of an array on backbearing determination.

The slowness vector resolution of different arrays can be compared using their "response" diagrams. The response diagrams of:

(i) the full EKA array;

(ii) two sub-arrays taken from the full array; and

(iii) the NORESS array

are shown in figure 23. The responses are plotted in terms of the zero lagged amplitude sum as a function of slowness in s/km for a 4 Hz signal. Multiplying the axes annotations by 4 (cycles per second) converts the diagrams to the more general unit of cycles/km. When plotted over the full range of likely slownesses for signals from near regional distances the response for the full array shows the strongly peaked main lobe with repititions or grating lobes at higher wave numbers expected from a cross array with regularly spaced seismometers. These features explain the spurious maxima encountered in section 2.2.2 when the full range of slowness (0.0-0.3 s/km) was searched to determine slowness vectors. At least 200 slowness vectors must be used to be sure that a maximum is not missed. The problem of the grating lobes remains however, even for arrays consisting of subsets of the full geometry, unless slowness ranges appropriate only to incoming P arrivals are considered. The advantage of the smaller arrays lies in the much broader maxima which requires fewer beams to guarantee its detection, unfortunately there is an inevitable loss of resolution and S/N gain.

To evaluate the location capability actually achieved by the array the measured backbearings to the 58 seismic sources studied were compared with those calculated from independent estimates of the epicentres. For quarry blasts the true epicentres are known but for earthquakes the epicentres were taken from locations published in Bulletins of the International Seismological Centre and more recently from the Preliminary Catalogue of Earthquakes and Ground Disturbances of the British Geological Survey. Errors in these epicentres will tend to increase the apparent errors in the backbearing estimates but by how much is difficult to quantify. Most epicentres are probably located to within 5 km or better corresponding to backbearing errors of up to 1.5° at 200 km range. Some earthquakes in the North Sea may have much larger errors with corresponding backbearing errors up to perhaps 4°. The conclusions described below with regard to the errors in backbearings are therefore probably pessimistic.

Histograms of the backbearing errors found with beamforming using the mean power and mean interchannel correlation criteria for 1 and 2 s time windows are shown in figure 24. Also shown are the results obtained when maximising semblance where

$$\text{Semblance} = \frac{\sum_{k=1}^{M} \left(\sum_{i=1}^{N} s_i(k+t_i) \right)^2}{N \sum_{k=1}^{M} \sum_{i=1}^{N} s_i(k+t_i)^2} \qquad (5)$$

The semblance is similar to the mean correlation but is faster to compute. Figure 24 indicates that there is little to choose between the three beamforming criteria or time window lengths employed. About 12% of the backbearings obtained using the 1s window and maximising the power however had gross errors. The principal conclusion however is that the full EKA array can determine the backbearings of a set of epicentres drawn from a variety of locations with a standard deviation of 3.5°. Converted to transverse location error this corresponds to 6,18 and 36 km at epicentral distances of 100, 300 and 600 km respectively. If the subarray consisting only of the 6 elements nearest to the array arm crossover is used, then the backbearing errors are increased by 50% (figure 25). These compare favourably with those for the full array considering that there is a 4 to 5 fold reduction in aperture.

5. GENERAL CONCLUSIONS

The overall conclusions of the study are as follows.

(a) Average noise levels for the 20 EKA seismometer sites derived from 48 short samples taken during 1989 are 10 nm^2/Hz at 1 Hz falling to 5 x 10^{-4} nm^2/Hz at 8 Hz.

(b) Noise at frequencies below 0.33 Hz is well correlated across the array and comes predominently from the north west quadrant with an average slowness of 0.275 s/km (3.64 km/s). Within the 0.33-1 Hz band correlations are weaker and have the largest values for a wide range of northerly backbearings and have a minimum to the south. The mean observed slowness in the 0.33-1 Hz band is 0.291 s/km (3.44 km/s). The source of noise at these low frequencies is believed to be the surrounding seas. At 1-2 Hz the noise is uncorrelated over distances of the order of the EKA aperture but there is a significant correlation for adjacent seismometers 0.9 km apart. At higher frequencies the noise is effectively uncorrelated over distances equal to or greater than the EKA seismometer separation and the amplitude of any negative swing in the variation of noise correlation with seismometer separation is less than 0.05.

(c) Correlations of P waves from seismic disturbances, mainly within 500 km of EKA, are influenced by the window length used to obtain the appropriate alignment of the channels. This is probably caused by the presence of several different phase types within the window which also results in an increased scatter of mean correlations for the 90-250 km epicentral distance range. In general, correlations fall to 0.5 at seismometer separations of 2 and 3 horizontal wavelengths of the signal and for 2 s and 1 s windows respectively.

(d) There is some reduction in measured correlations when channels are aligned using only the slowness vector of the wavefront compared with those obtained if individual channel shifts (relative to the array sum) are introduced. These shifts are all small (<0.025 s) but for some channels their average values are significantly different from zero.

(e) S/N gains on beamformed signals from near-regional sources predicted from

the observed correlation data for the full array, average 3.8 in the 2-4 Hz band and fall to 3.0 in the 6-8 Hz band. Smaller aperture arrays with the same number of seismometers could achieve slightly higher gains and the array sum would better preserve the signal spectrum.

(f) The presence of grating lobes in the array response result in frequent errors in the estimated slowness vectors of signals from local and near-regional seismic disturbances when beam optimisation permits slowness values as high as 0.33 s/km corresponding to crustal S waves. This problem is greatest when optimising for mean power and using short (0.5 s) time windows. It is reduced when using measures of correlation for beam optimisation and with longer (1-2 s) time windows. Use of the slowness range corresponding to P waves (0.0-0.2 s/km) is effective in removing the problem.

(g) Backbearings determined for P arrivals with good S/N ratio have standard errors of 3.4 to 4.0° when using data from the full array. These errors increase to 5.1-6.4° when only the central 6 seismometer subarray is used.

Although the 2-8 Hz frequency band considered in this report is recorded using a digital sampling rates of 20 samples/s it is important to note that the channel alignments necessary to make use of the full array capabilities require much shorter relative shifts than 0.05 s. Hence a higher sampling rate than 20 samples/s or an interpolation scheme is necessary for beamforming of signals in the 2-8 Hz band.

6. ACKNOWLEDGEMENTS

The author would like to thank the staff at Blacknest and in particular Mrs P Peachell for her efforts in digitising the analogue data. Thanks also to the staff of EKA for maintaining the data acquisition, the many quarry owners for information on the location of many of the sources used in this study and also the British Geological Survey for copies of their Preliminary Bulletin of UK Seismic Events.

REFERENCES

1. Key, F A, Marshall, P D and A J McDowall. "Two Recent British Earthquakes Recorded at the UK Atomic Energy Authority Seismometer Array at Eskdalemuir". Nature, 201, 4918, 484-485 (1964).

2. Cleary, J. "Array and Multi-Station Analysis of an Earthquake in Cornwall: A Comparative Study". Geophys J R Astr Soc, 12, 437-441 (1966).

3. Birtill, J W and F E Whiteway. "The Application of Phased Arrays to the Analysis of Seismic Body Waves". Phil Trans Roy Soc, 1091, 258, 421-493 (1965).

4. Mykkeltveit, S, Astebol, K, Doornbos, D J and E S Husebye. "Seismic Array Configuration Optimisation". Bull Seism Soc Am, 73, 173-186 (1983).

5. Bache, T C, Marshall, P D and J B Young. "High Frequency Seismic Noise Characteristics at the Four United Kingdom-Type Arrays". Bull Seism Soc Am, 76, 3, 601-616 (1986).

6. Douglas, A and J B Young. "The Estimation of Seismic Body Wave Signals in the Presence of Oceanic Microseisms". AWRE Report No. 0 14/81, HMSO (London) (1981).

7. Geller, R J and C S Mueller. "Four Similar Earthquakes in Central California". Geophysical Research Letters, 7, 821-824 (1980).

8. Thorbjarnardottir, B S and J C Pechmann. "Constraints on Relative Earthquake Locations from Cross-Correlation of Waveforms". Bull Seis Soc Am, 77, 5, 1626-1634 (1987).

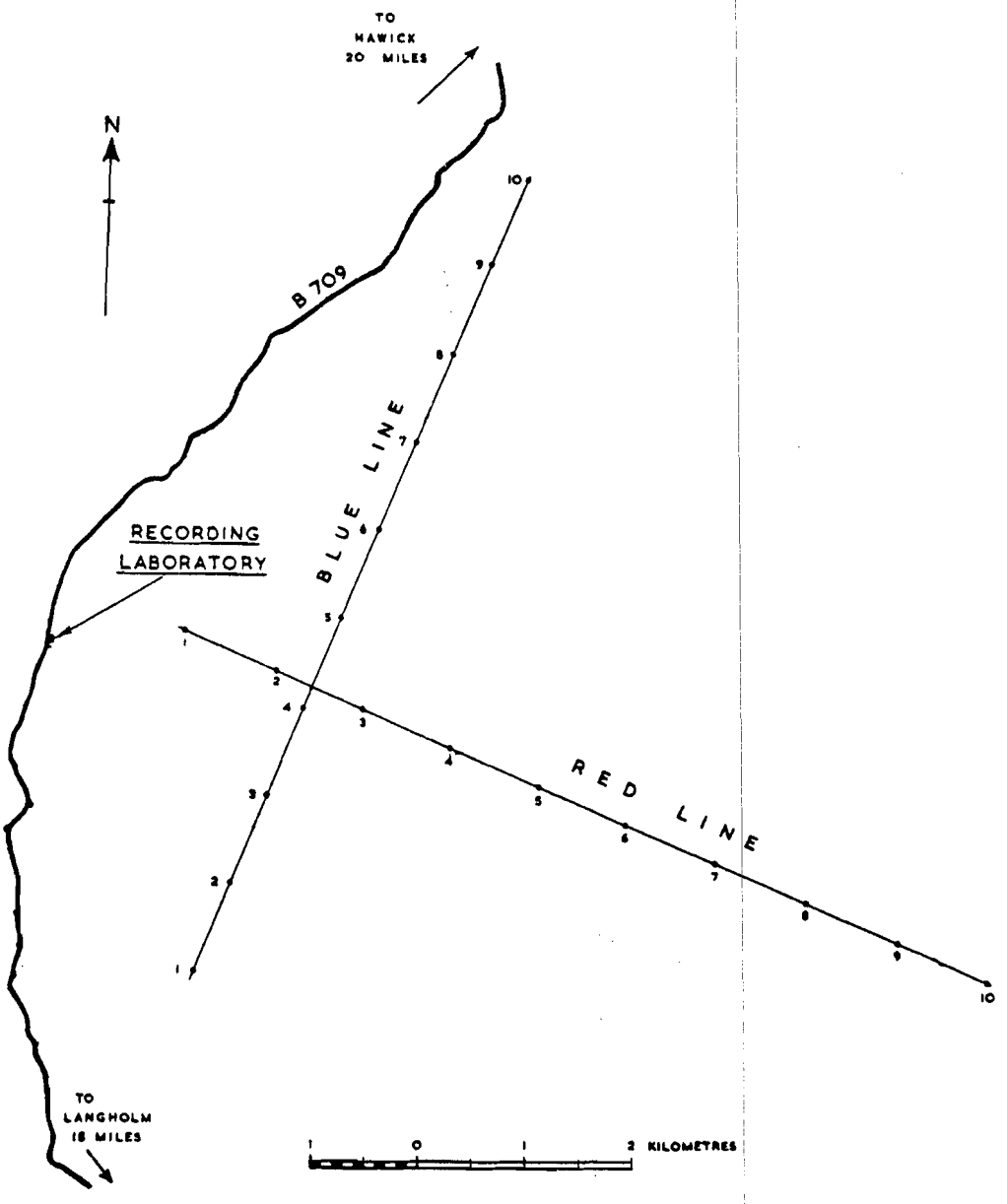

Figure 1 Map showing seismometer locations of the Eskdalemuir array EKA. In the text seismometers are referred to as R1–R10 and B1–B10 for the Red and Blue lines respectively.

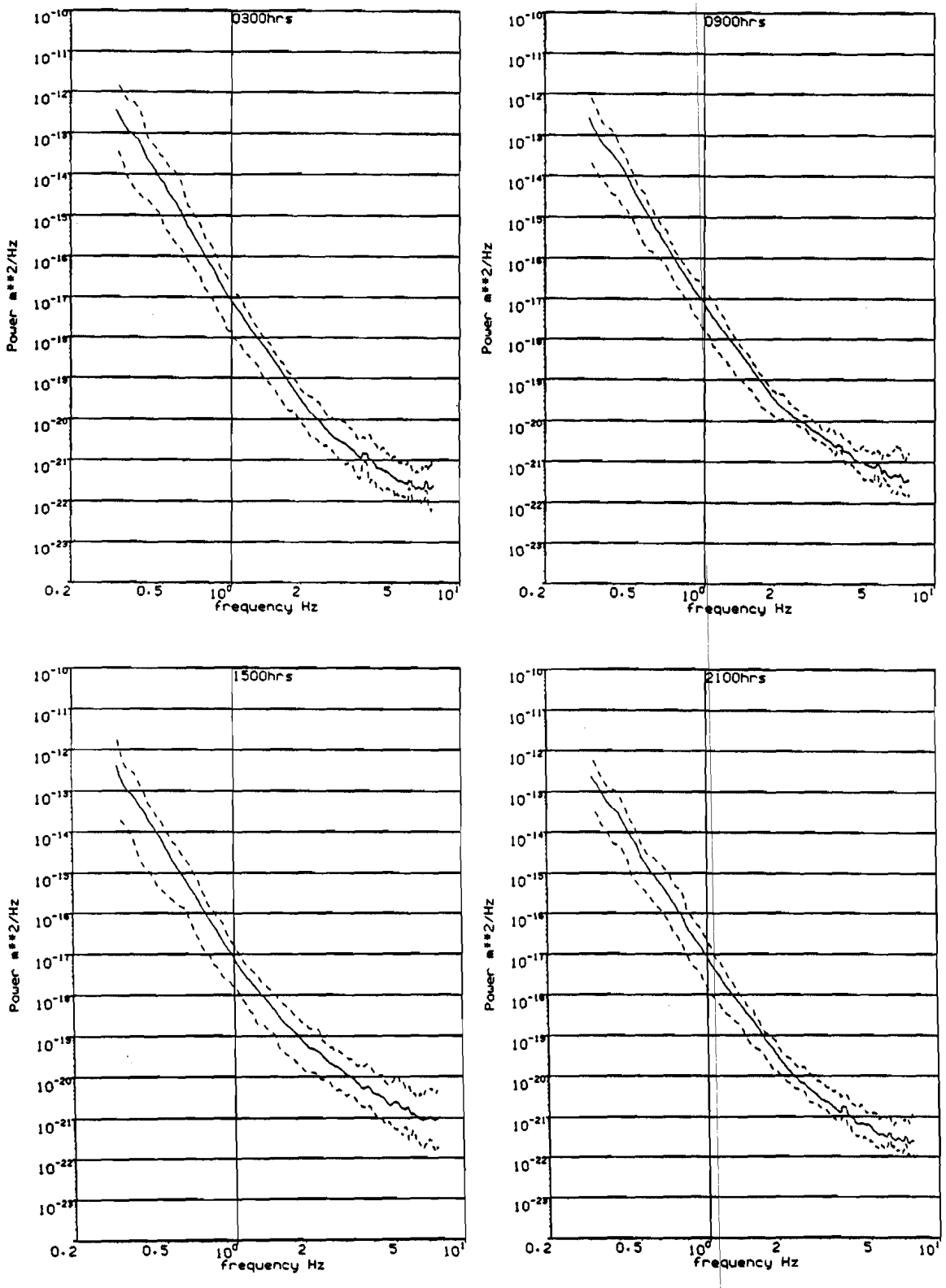

Figure 2 Power spectra for noise samples taken at 0300,0900,1500 and 2100 hours GMT on 12 days during 1989. The solid curve represents the average of twelve twenty channel spectra stacks (one sample on one day from each of twelve months). The dashed curves represent the maximum and minimum values of the 12 stacks.

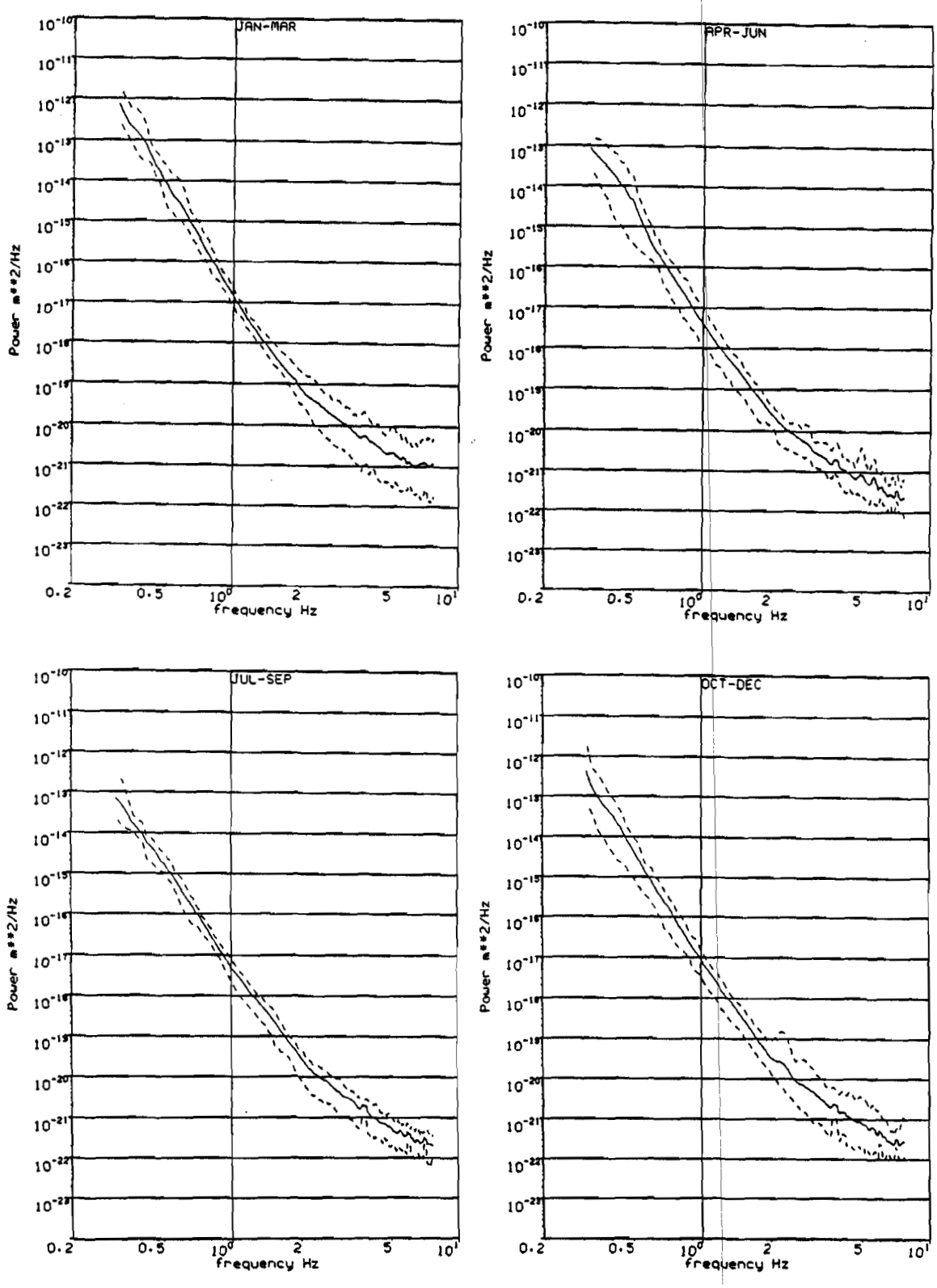

Figure 3 Power spectra for noise samples taken during JAN–MAR, APR–JUN, JUL–SEP and OCT–DEC 1989. The solid curves represent the average of twelve twenty channel spectra stacks (four samples during one day from each of three months). The dashed curves are the maximum and minimum values of the twelve stacks.

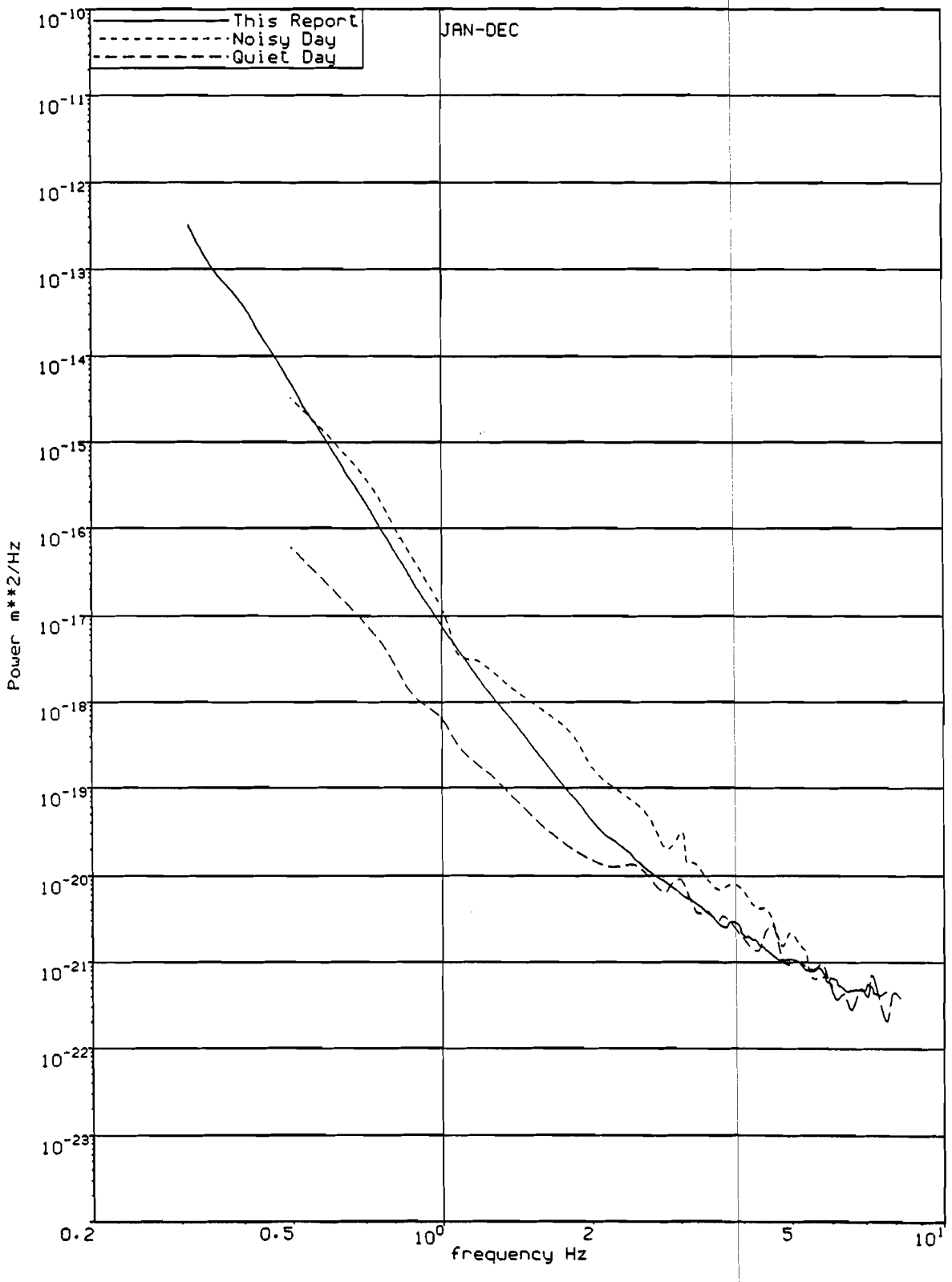

Figure 4 Power spectra for noise samples taken during 1989 compared with spectra published by Bache, Marshall & Young (5) for EKA. The solid curve represents the average of forty eight twenty channel spectra stacks (samples four times per day for one day per month). The dashed curves are the 'noisy day' and 'quiet day' spectra published in Bache et al (5).

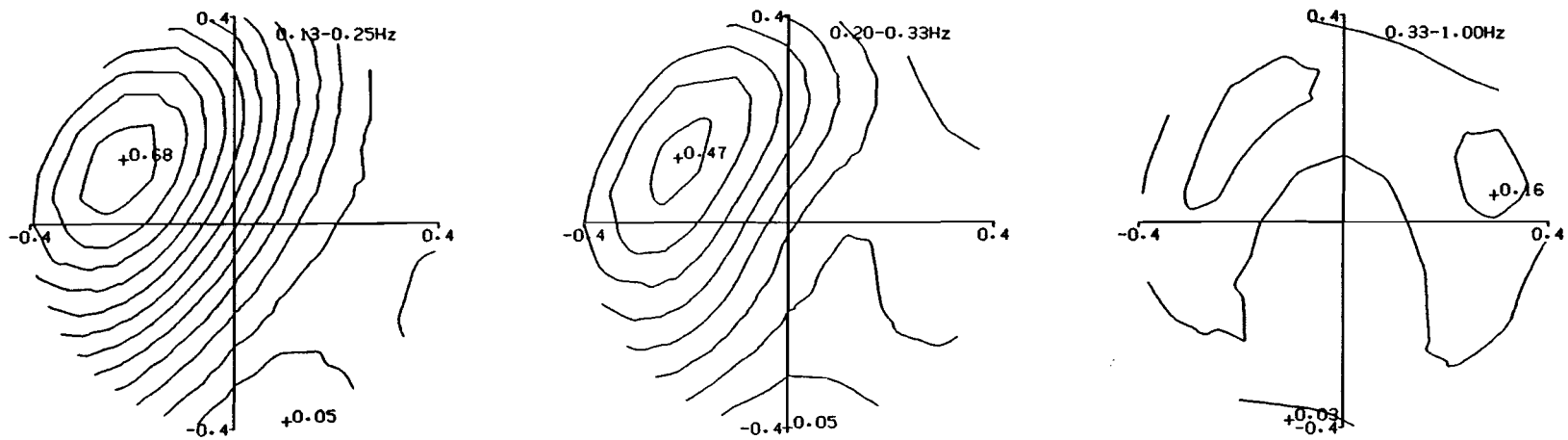

Figure 5 Mean interchannel correlation of 48 noise samples taken in 1989 for EKA. The results for 3 frequency bands are shown. The mean correlation is contoured at intervals of 0.05 as function of slowness in s/km and the maximum and minimum values marked. In the lower two frequency bands the noise is highly correlated and arrives on average from the NW. The noise is considerably less well correlated in the 0.33–1.0 Hz band and appears more isotropic. The North Sea is a possible additional noise source.

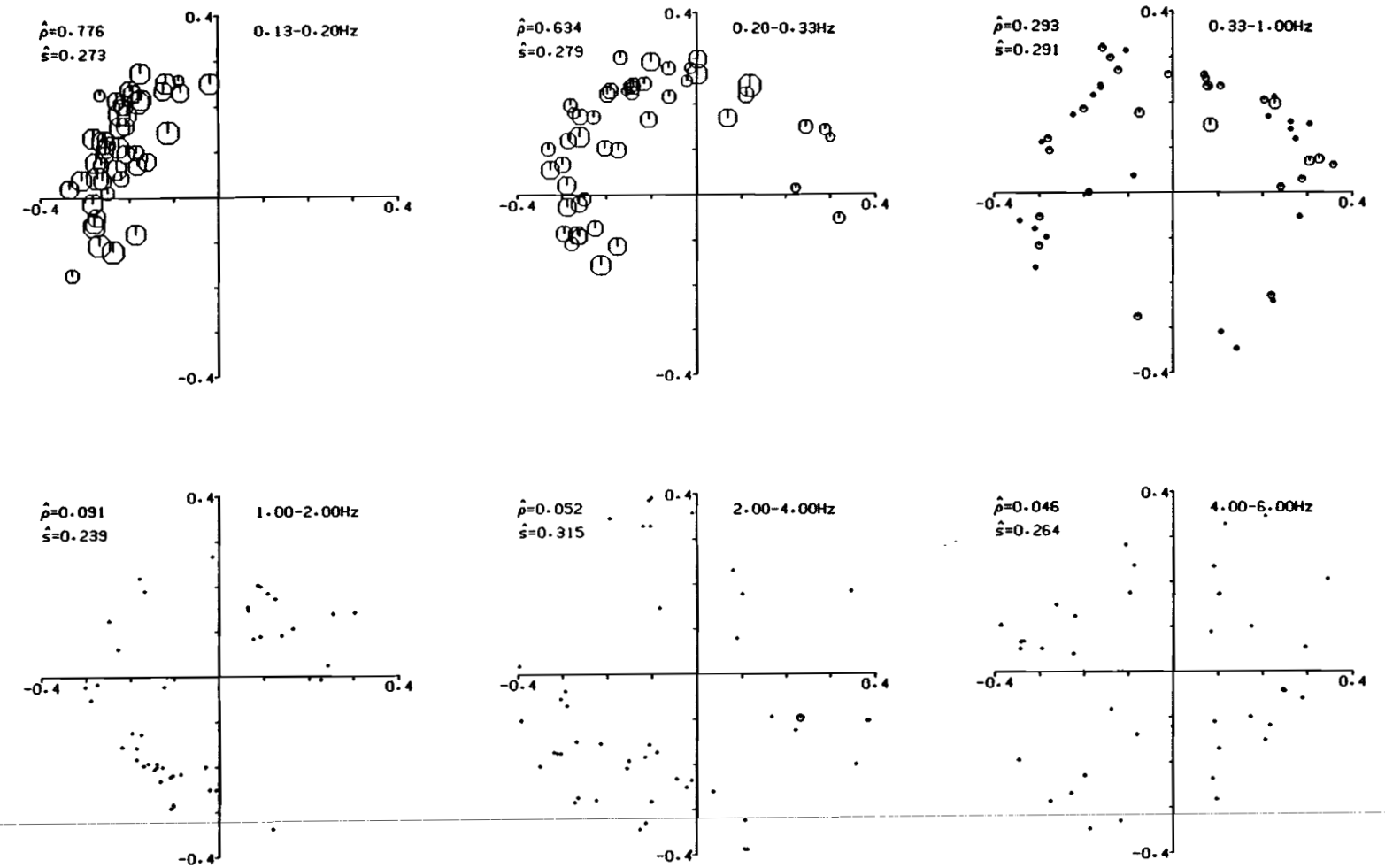

Figure 6 Plots showing the slowness vectors giving the maximum mean iter channel correlation for each of forty eight noise samples taken in 1989 for EKA. The results for six frequency bands are shown. The symbol size is proportional to the correlation. The overall mean correlation and slowness are given in the top left. For the 0.13–0.25 and 0.20–0.33 Hz bands the noise is well correlated and generally arrives from the NW quadrant at slowness corresponding to a speed of 3.6km/s. In the 0.33–1 .Hz band the correlations are much lower, directions more isotropic and speed slightly lower at 3.4km/s. At higher frequencies the noise appears to be uncorrelated.

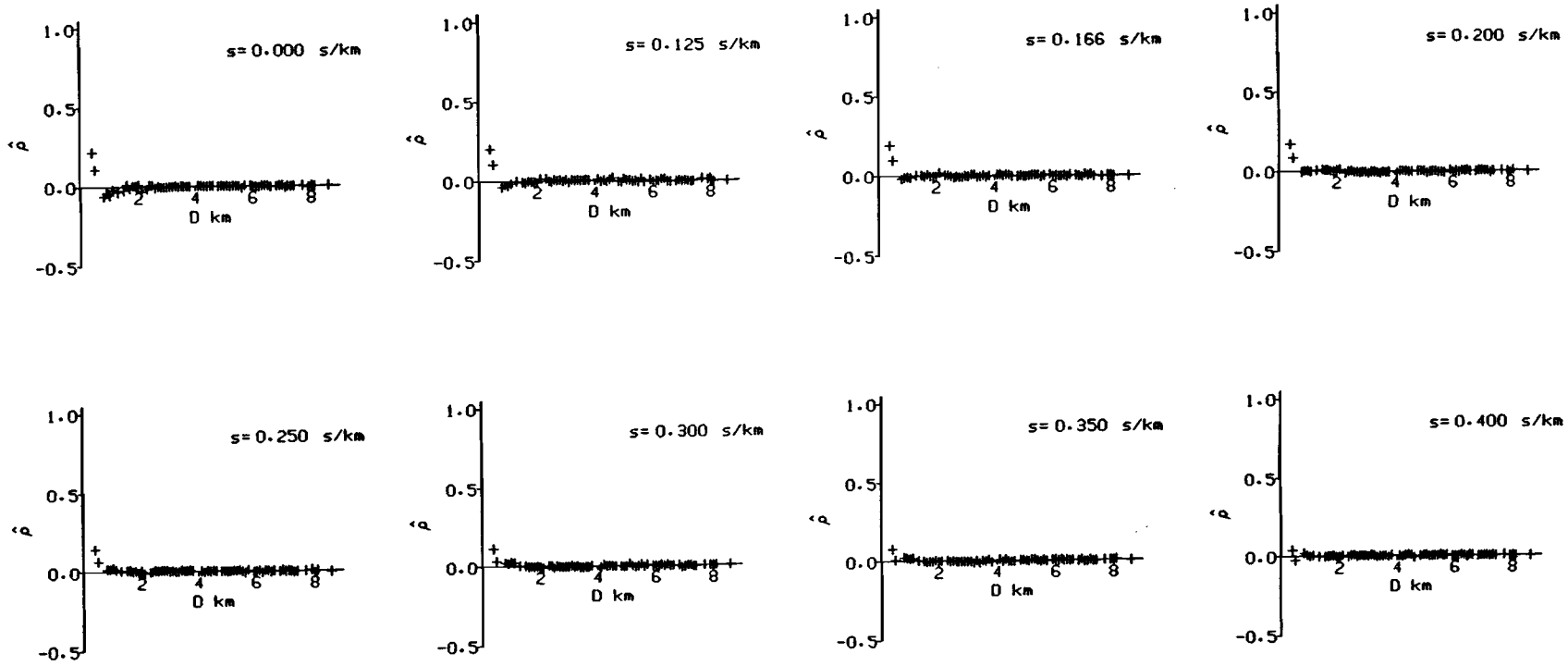

Figure 7 Plots of inter channel noise correlation ρ_{ij} against seismometer separation D for the frequency band 2–4 Hz. Each plot corresponds to a different slowness s. Each point represents the average $\hat{\rho}$ over 48 noise samples and a range of backbearings. The averages $\hat{\rho}$ are computed with the data grouped into 0.1km distance cells. The noise is uncorrelated at separations greater than 1km and becomes positively correlated at less than about 0.5km. Any negative excursion between 0.5–1km separation appears to be less than 0.05 amplitude.

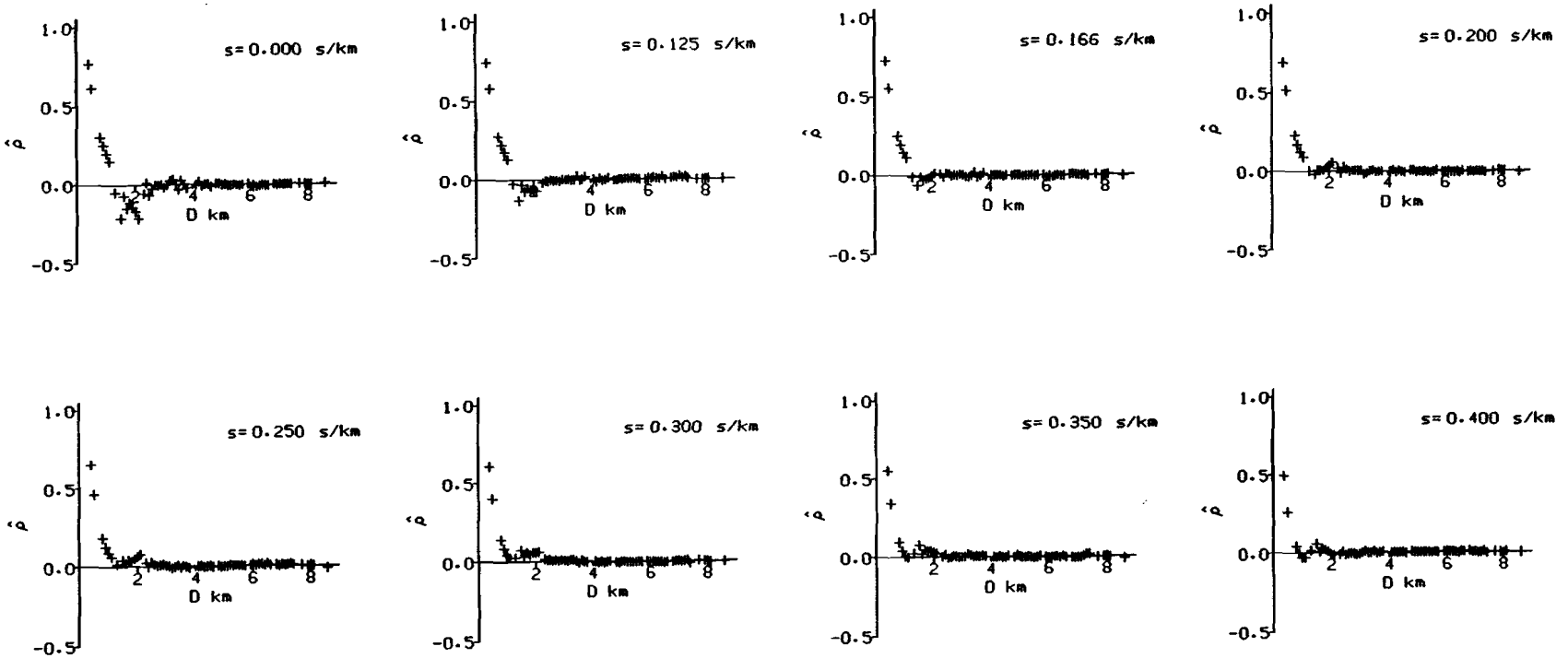

Figure 8 Plots of interchannel noise correlation ρ_{ij} against seismometer separation D for the frequency band 1–2 Hz. Each plot corresponds to a different slowness s. Each point represents the average $\hat{\rho}$ over 48 noise samples and a range of backbearings. The averages $\hat{\rho}$ are computed with the data grouped into 0.1km distance cells. The noise is uncorrelated at separations greater than 2.5km and becomes positively correlated at less than about 1.5km. Variations between the plots indicates that the noise is not entirely isotropic in slowness.

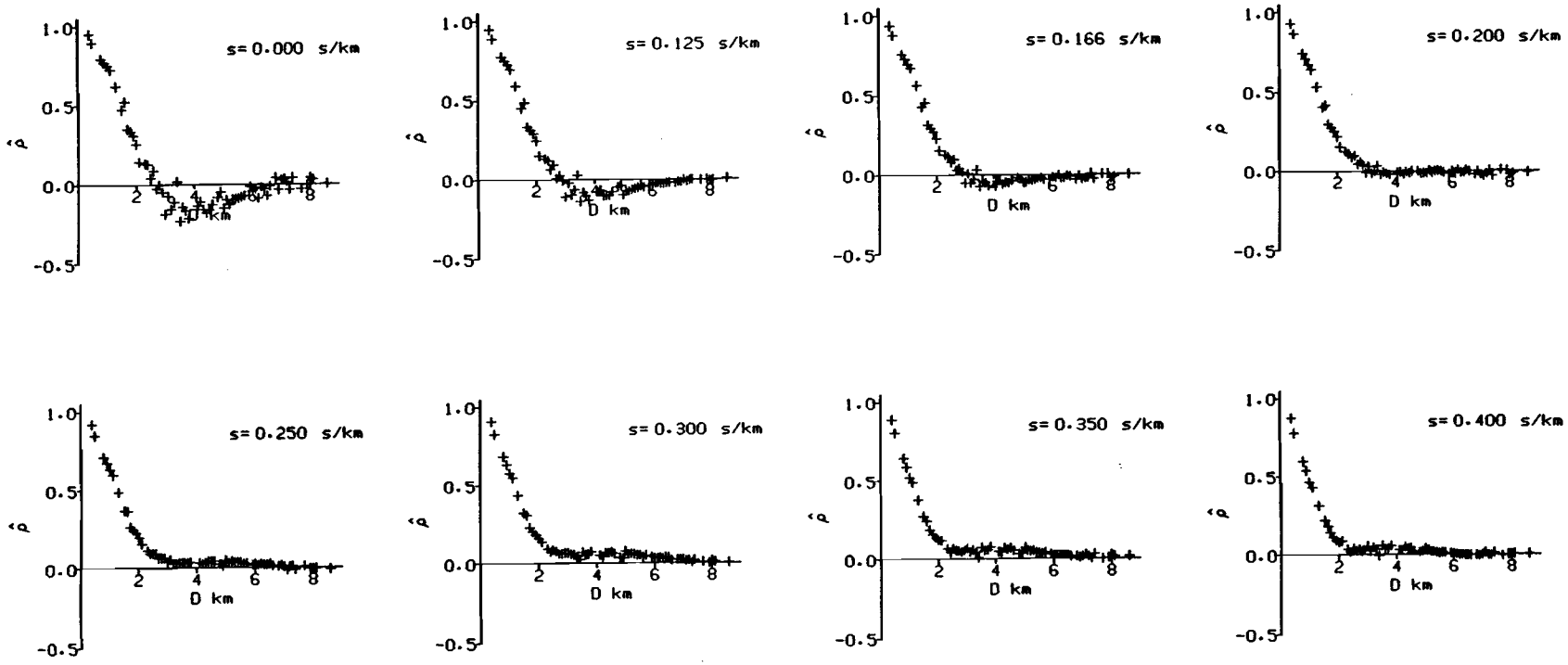

Figure 9 Plots of inter channel noise correlation ρ_{ij} against seismometer separation D for the frequency band 0.33–1 Hz. Each plot corresponds to a different slowness s. Each point represents the average $\hat{\rho}$ over 48 noise samples and a range of backbearings. The averages $\hat{\rho}$ are computed with the data grouped into 0.1km distance cells. The noise is positively correlated at separations less than 3km and variations between the plots indicate the presence of some anisotropy in slowness.

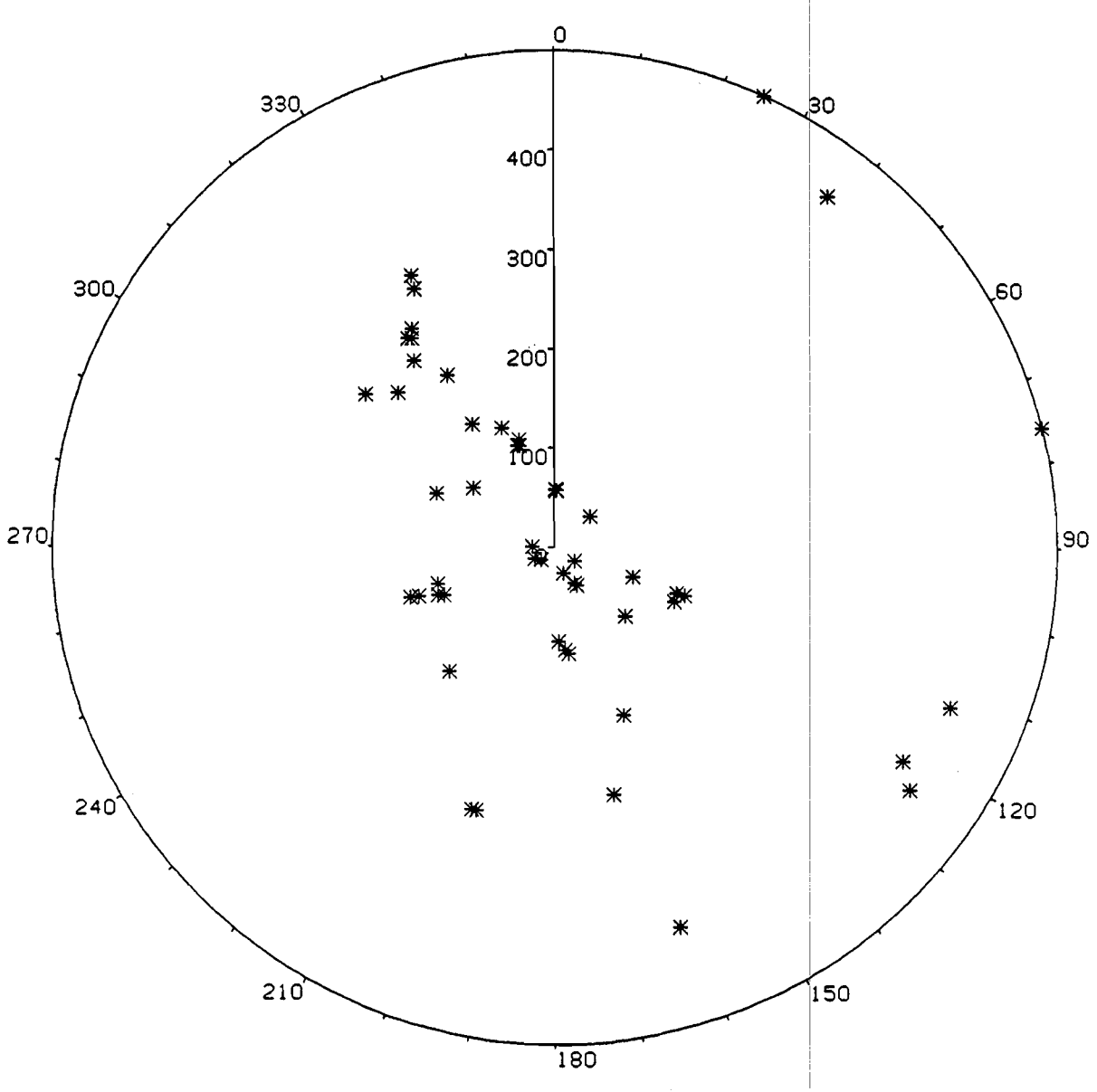

Figure 10 Epicentre distribution of seismic disturbances used in this study centred on EKA and out to 500km distance. Note that two epicentres plotted on the periphery are at distances in excess of 500km

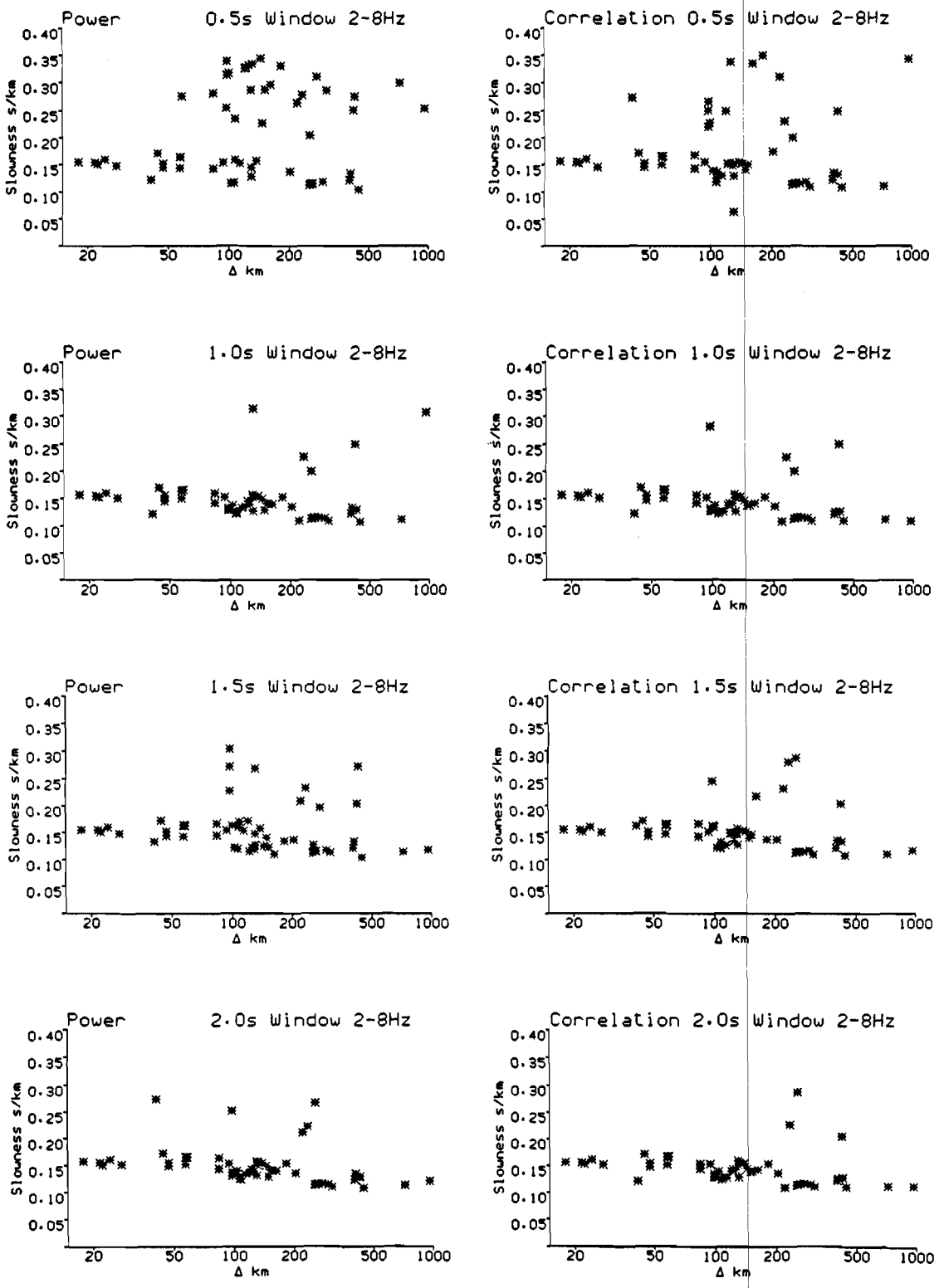

Figure 11 Plots of slowness determined by EKA against epicentral distance. The data used are 2–8 Hz bandpass filtered and beams formed for time windows of 0.5,1.0,1.5 and 2.0 seconds length starting at the P wave onset. The results on the left are obtained by maximising the mean power of the array sum for each window and on the right by maximising the mean inter channel correlation. The search for the optimum beam included the full range of likely slowness 0.0–0.33s/km for local P and S wave arrivals. Many of the determined slowness values are too high for P waves and result from the convergence on spurious maxima arising from side lobes in the array response.

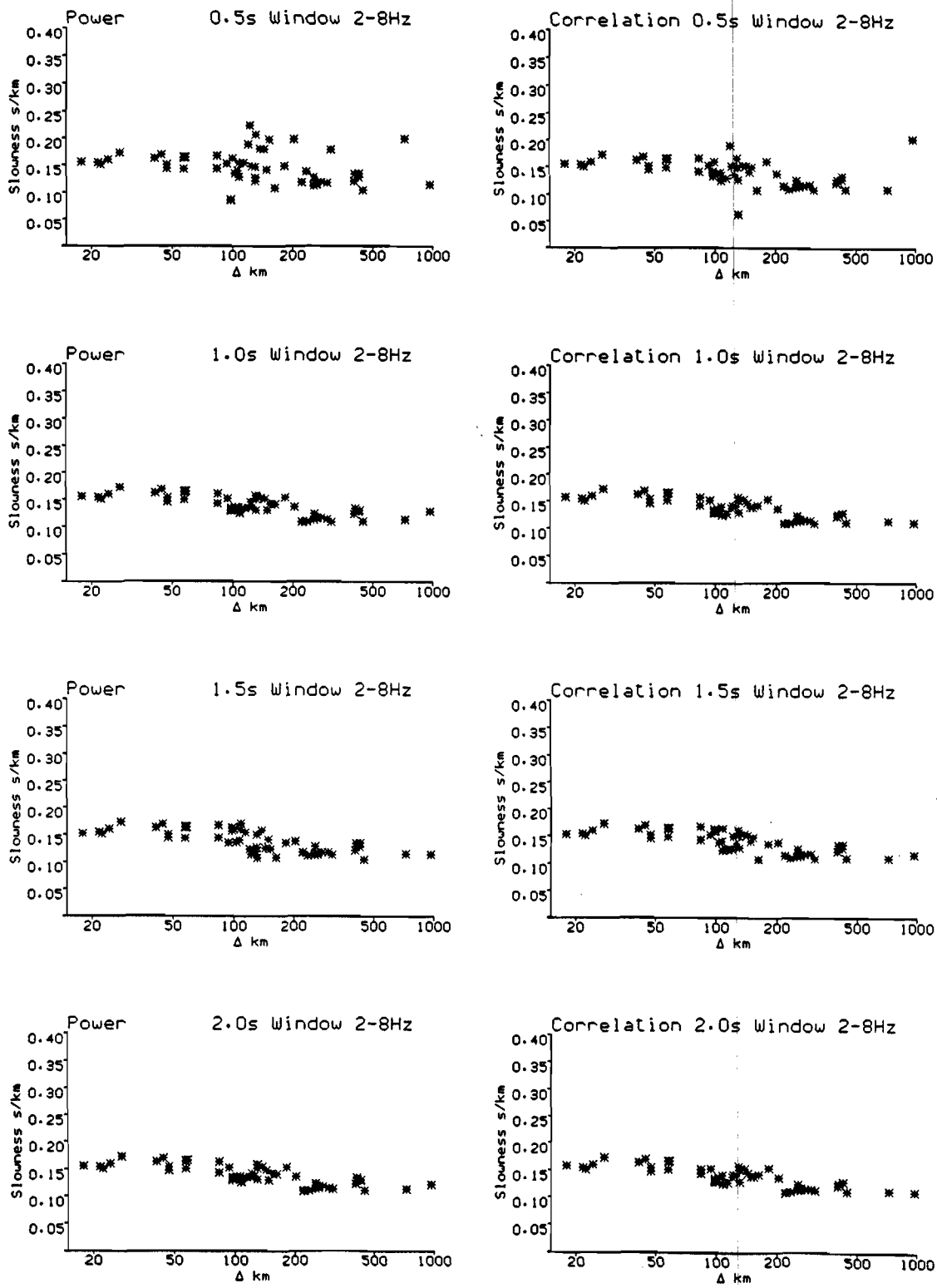

Figure 12 Plots of slowness determined by EKA against epicentral distance.The data used are 2–8 Hz bandpass filtered and beams formed for time windows of 0.5,1.0,1.5 and 2.0 seconds length starting at the P wave onset. The results on the left are obtained by maximising the mean power of the array sum for each window and on the right by maximising the mean inter-channel correlation. The search for the optimum beam included only the range of slowness 0.0–0.2 s/km appropriate for local P wave arrivals. The spurious values visible in fig 11 have been eliminated and apart from some scatter when using the shortest (0.5s) window, the plots all show a general decrease in slowness over the 90–250km distance range

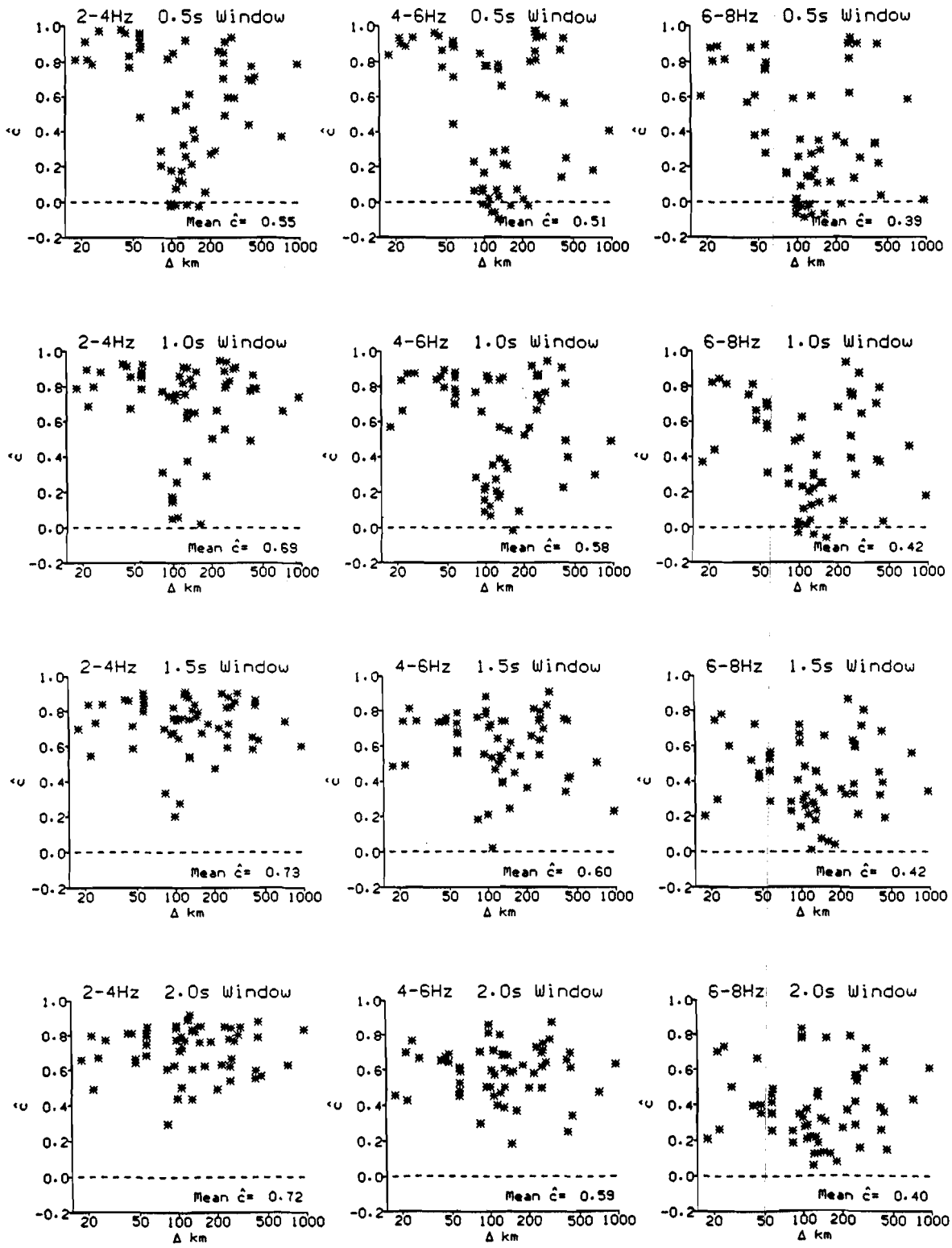

Figure 13 Mean inter channel correlation $\hat{c}$ plotted against epicentral distance of signals from 58 local and near regional seismic disturbances. Results using four time windows (0.5, 1.0, 1.5 & 2.0s) and three frequency bands (2–4,4–6 & 6–8Hz) are shown. In all cases correlations are computed using channel allignments based on slowness vectors determined by maximising the mean correlation for a 2 second window. The overall mean correlation for all the signals is given in the bottom right of each graph.

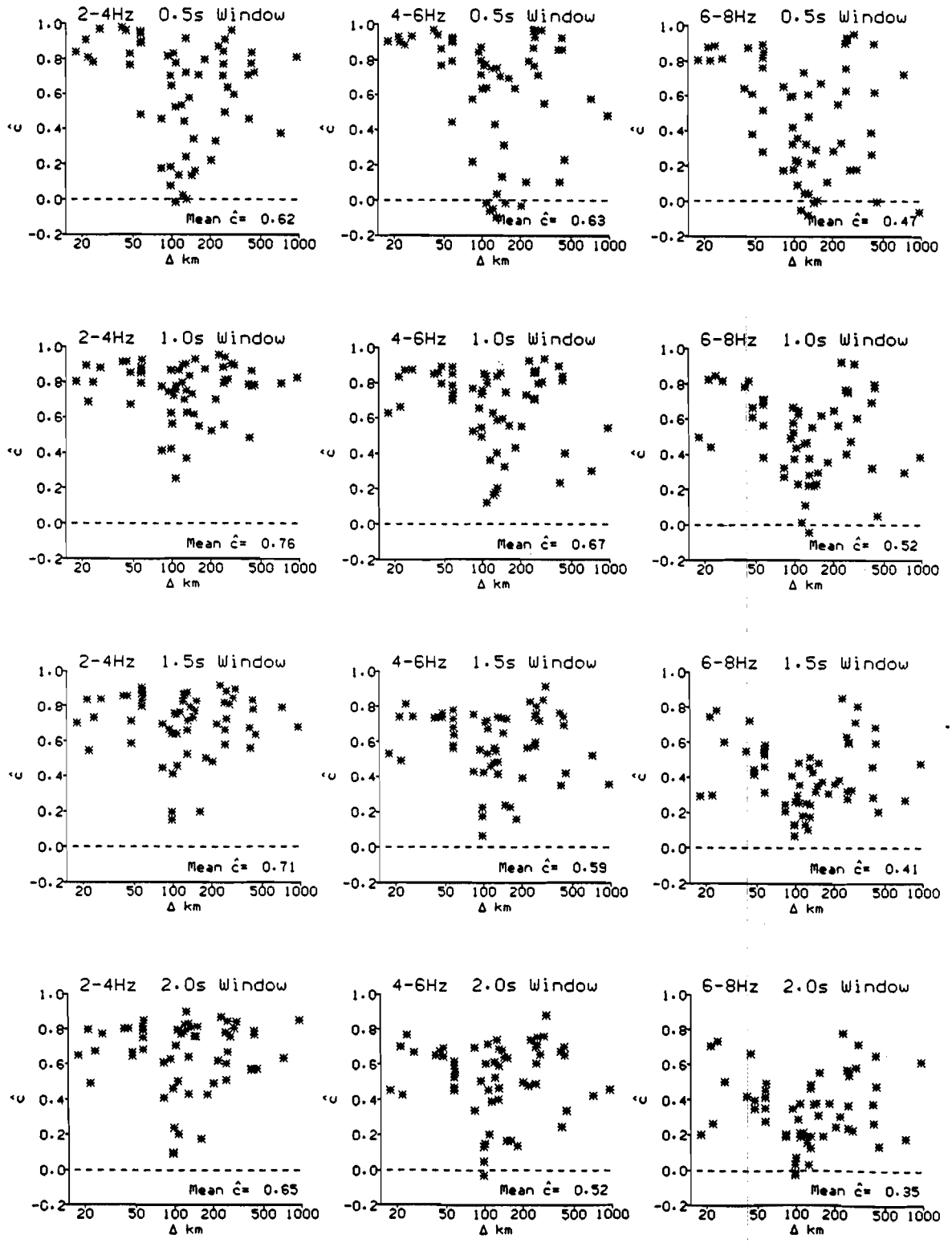

Figure 14 Mean inter channel correlation $\hat{c}$ plotted against epicentral distance of signals from 58 local and near regional seismic disturbances. Results using four time windows (0.5, 1.0, 1.5 & 2.0s) and three frequency bands (2–4,4–6 & 6–8Hz) are shown. In all cases correlations are computed using channel allignments based on slowness vectors determined by maximising the mean correlation for a 1 second window. The overall mean correlation for all the signals is given in the bottom right of each graph.

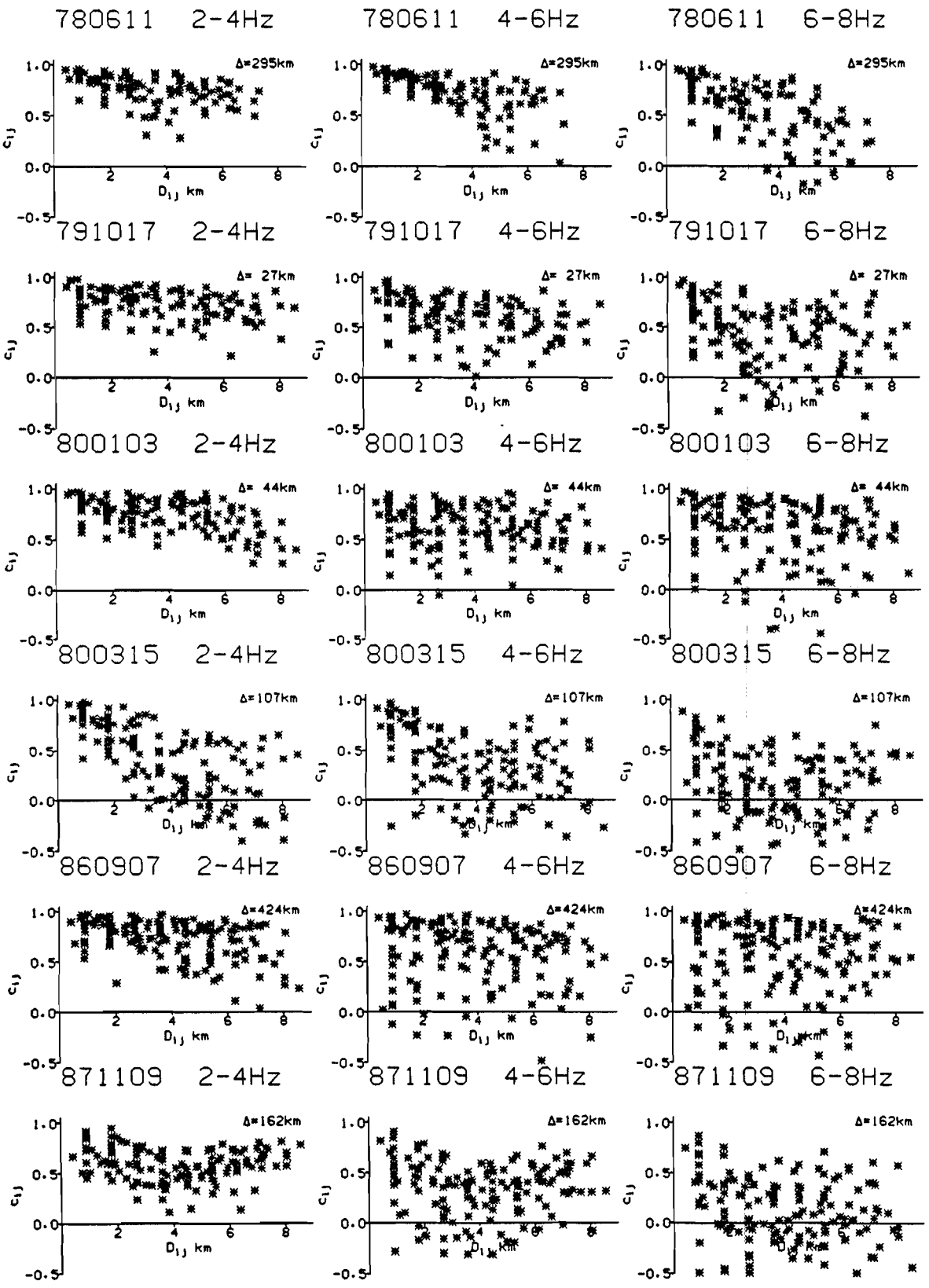

Figure 15 Inter-channel correlations c_{ij}, for a selection of seismic disturbances at various epicentral distances from EKA, plotted against the seismometer separation D_{ij}. Results for three frequency bands (2-4,4-6 & 6-8 Hz) are shown. Correlations are computed for a 2 second time window starting at the P wave onset.

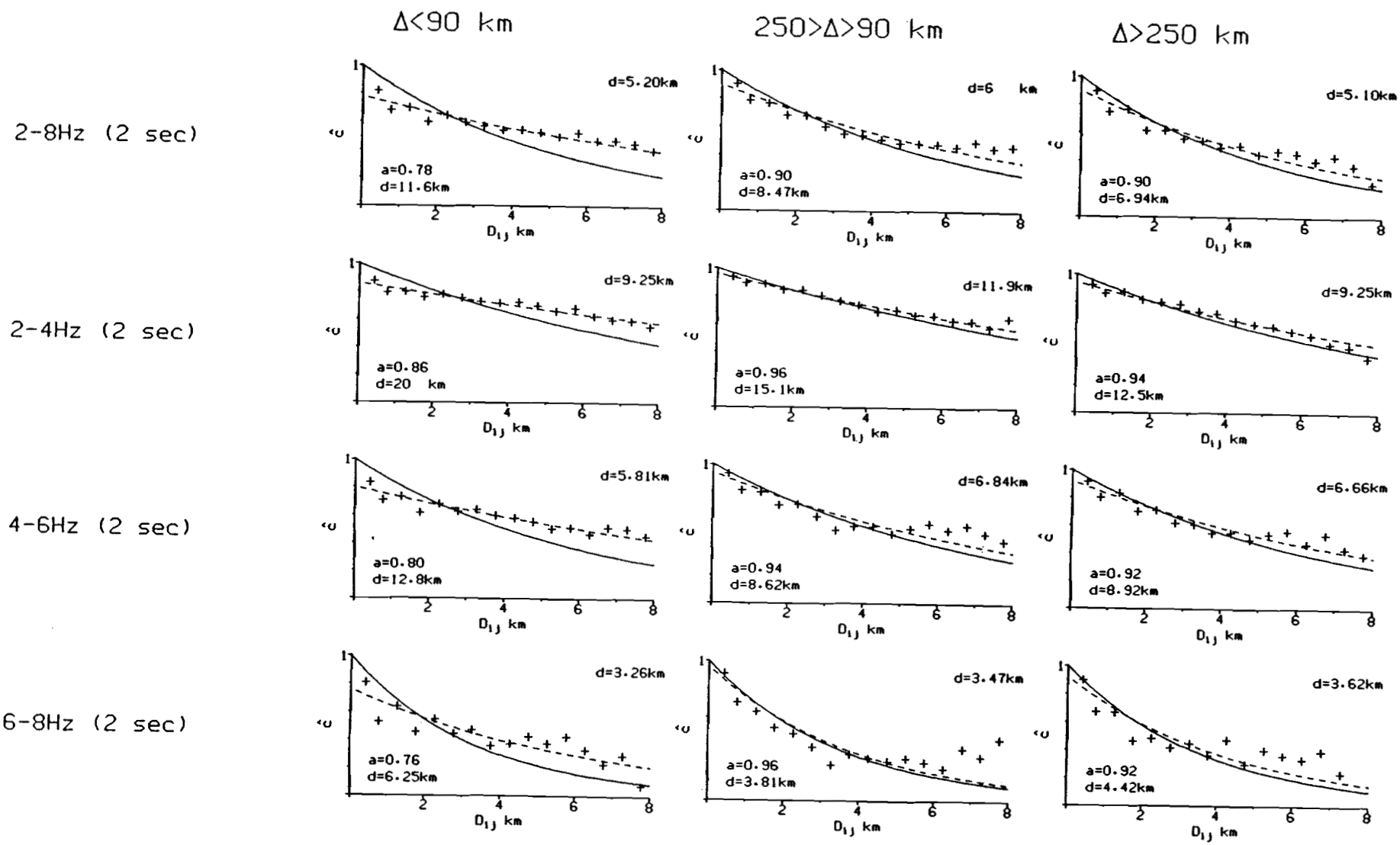

Figure 16 Mean inter channel correlation $\hat{c}$ of P wave signals plotted against seismometer separation D_{ij}. Correlations are computed after alligning the channels using slowness vectors obtained by maximising the mean correlation for a 2 second window and 2–8Hz bandpass. The points plotted are the average of 2 second window correlation values grouped into 0.5km distance cells. The solid curves, fitted to the points by least squares, have the form $c=e^{-D/d}$ where d is given in the top right of each graph. The dashed curves have the form $c=ae^{-D/d}$ where d and a are given in the lower left of each graph. The graphs are for data from three epicentral distance ranges and using 4 frequency bands as indicated at the top and left of the figure respectively.

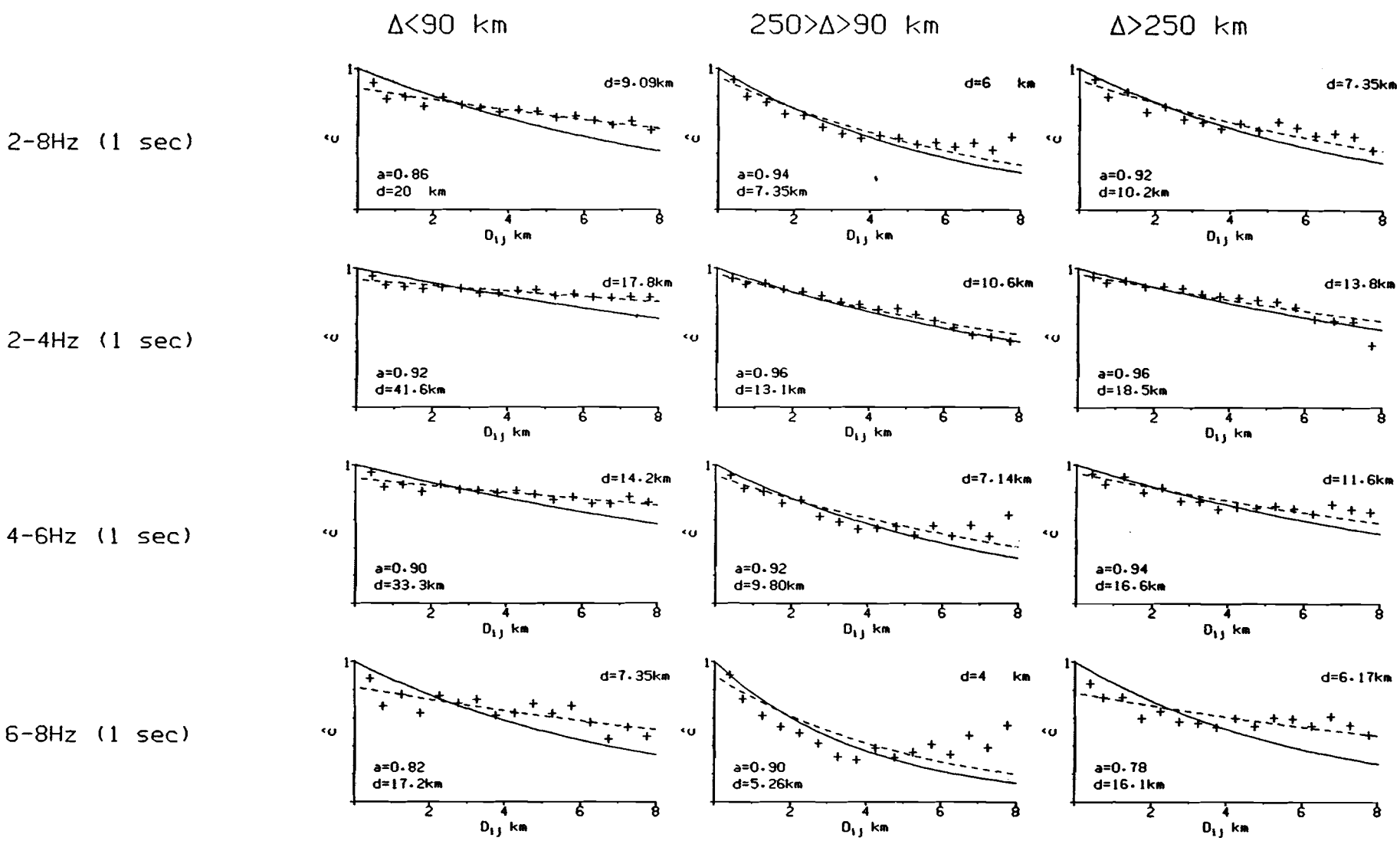

Figure 17 Mean inter channel correlation $\hat{c}$ of P wave signals plotted against seismometer separation D_{ij}. Correlations are computed after alligning the channels using slowness vectors obtained by maximising the mean correlation for a 1 second window and 2–8Hz bandpass. The points plotted are the average of 1 second window correlation values grouped into 0.5km distance cells. The solid curves, fitted to the points by least squares, have the form $c=e^{-D/d}$ where d is given in the top right of each graph. The dashed curves have the form $c=ae^{-D/d}$ where d and a are given in the lower left of each graph. The graphs are for data from three epicentral distance ranges and using 4 frequency bands as indicated at the top and left of the figure respectively.

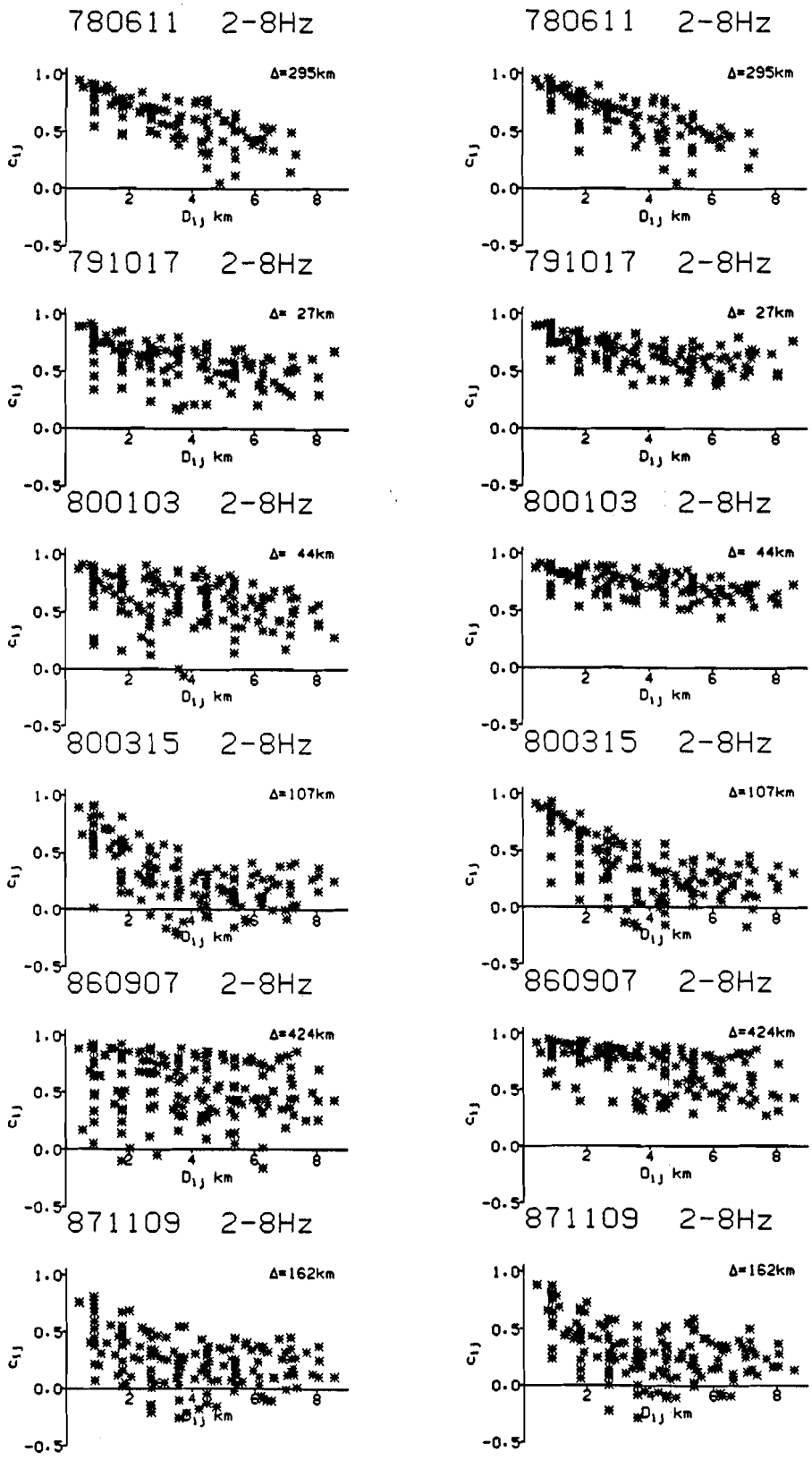

Figure 18 Inter channel correlations c_{ij}, for a selection of seismic disturbances at various epicentral distances from EKA, plotted against the seismometer separation D_{ij}. Results for the 2–8 Hz frequency band are shown. The correlation plots on the left hand side are obtained for a 2 second time window starting at the P wave onset and using channel allignments based on slowness vectors which maximise the mean inter–channel correlation. The correlations on the right are obtained after using additional shifts in an attempt to achieve improved allignments. These shifts are obtained by first forming the array sum for the existing channel allignments and then finding the relative shift which maximises the cross correlation of the sum with each channel.

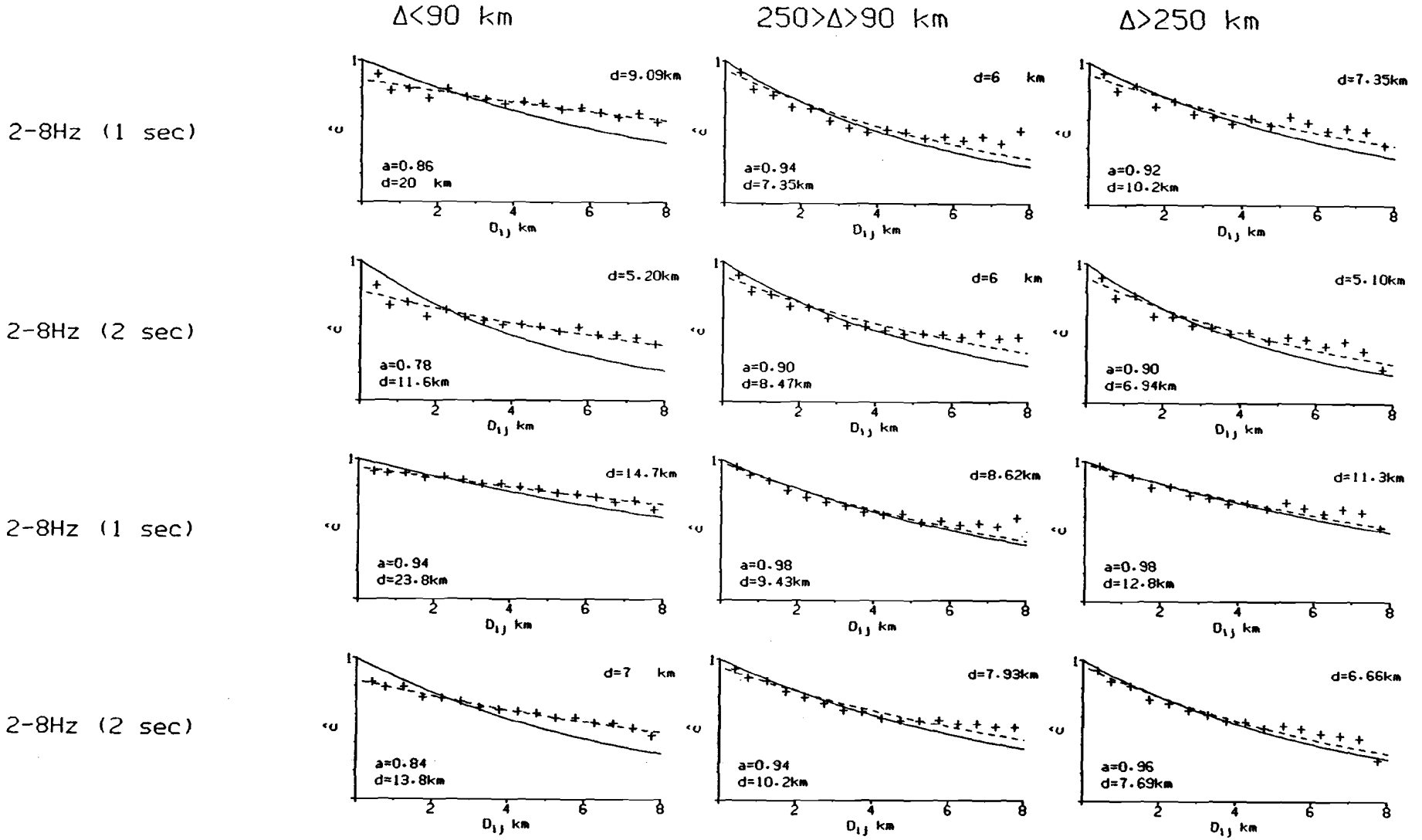

Figure 19 Mean inter channel correlation $\hat{c}$ *of P wave signals plotted against seismometer separation* D_{ij}. The points plotted are the average correlation values grouped into 0.5km distance cells. The solid curves, fitted to the points by least squares, have the form $c=e^{-D/d}$ where d is given in the top right of each graph. The dashed curves have the form $c=ae^{-D/d}$ where d and a are given in the lower left of each graph. The graphs are for data from three epicentral distance ranges and using a 2–8Hz frequency band with correlations over 1 or 2 second time windows as indicated at the top and left of the figure respectively. Correlations in the top two rows were computed using channel allignments based on slowness vectors only. In the bottom two rows additional relative shifts have been used to improve channel allignment..

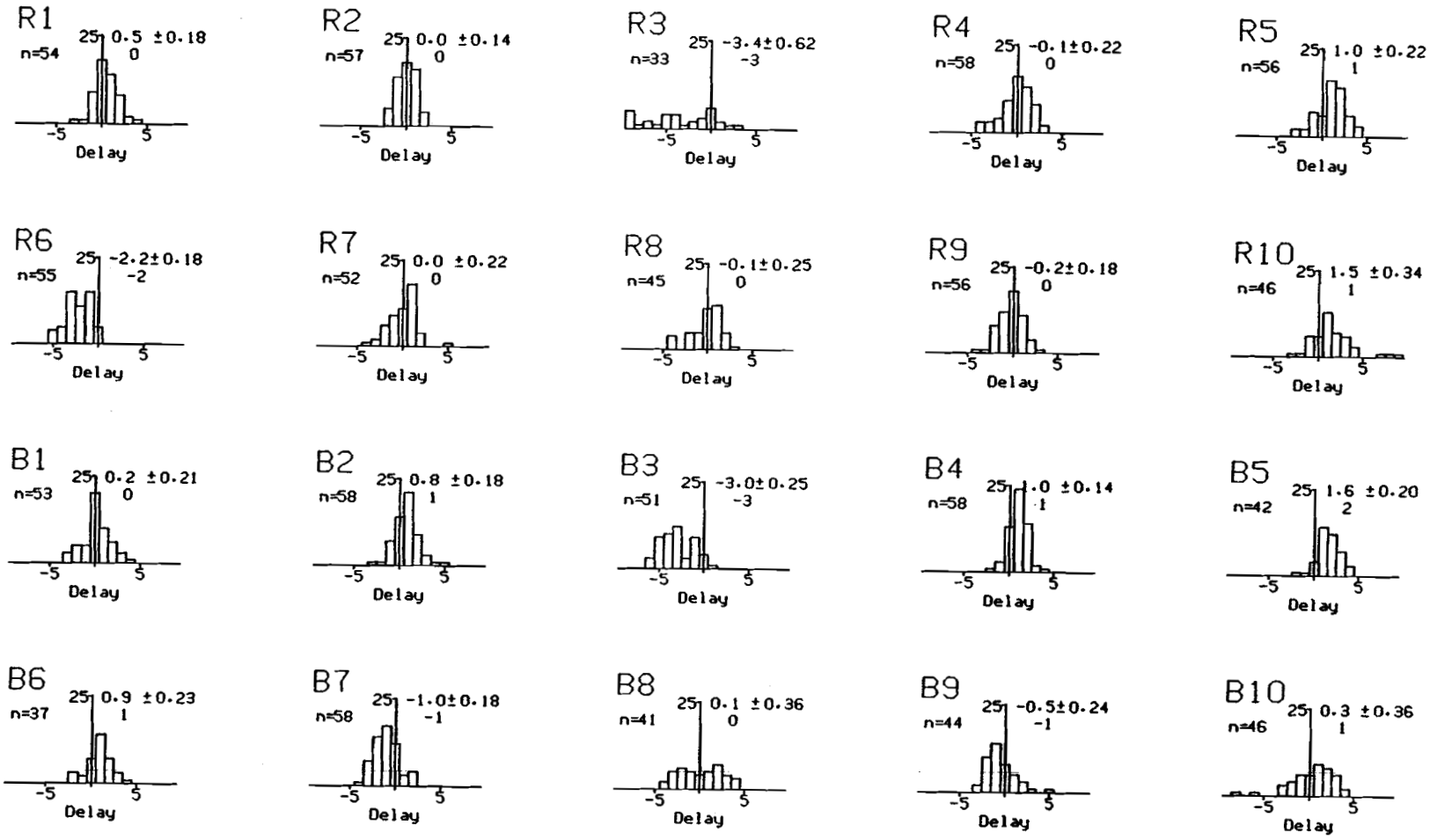

Figure 20 Histograms showing the distribution of relative delays required to optimise channel allignmemts for the 58 seismic disturbances studied and the 20 channels of EKA. The delays are in units of 1 sample for a rate of 160 per second. On the top right of each histogram is the number of conributing values n. On the left are the mean value with its standard deviation and the median delay in samples.

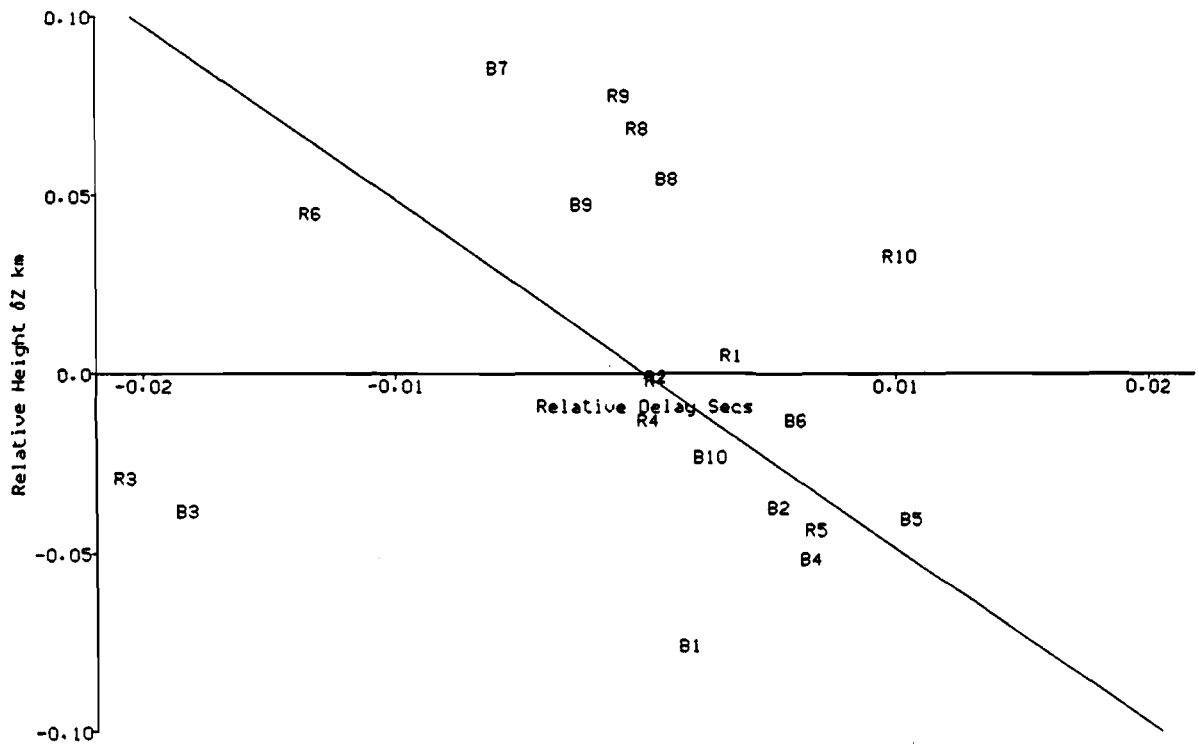

Figure 21 Mean relative channel delays plotted against relative heights of the seismometers. The straight line represents the correction to allow for Relative height δZ given by $-\delta Z*\cos(i)/V$ with $\sin(i)=V/V_a$. V is the surface P wave speed (assumed =4.0km/sec) and V_a is the apparent velocity of the incoming wavefront (assumed =7.0km/sec). Note that a positive delay here means that the observed time series must be moved later in time and for a negative delay moved earlier to allign the channels. Height Z is positive upwards.

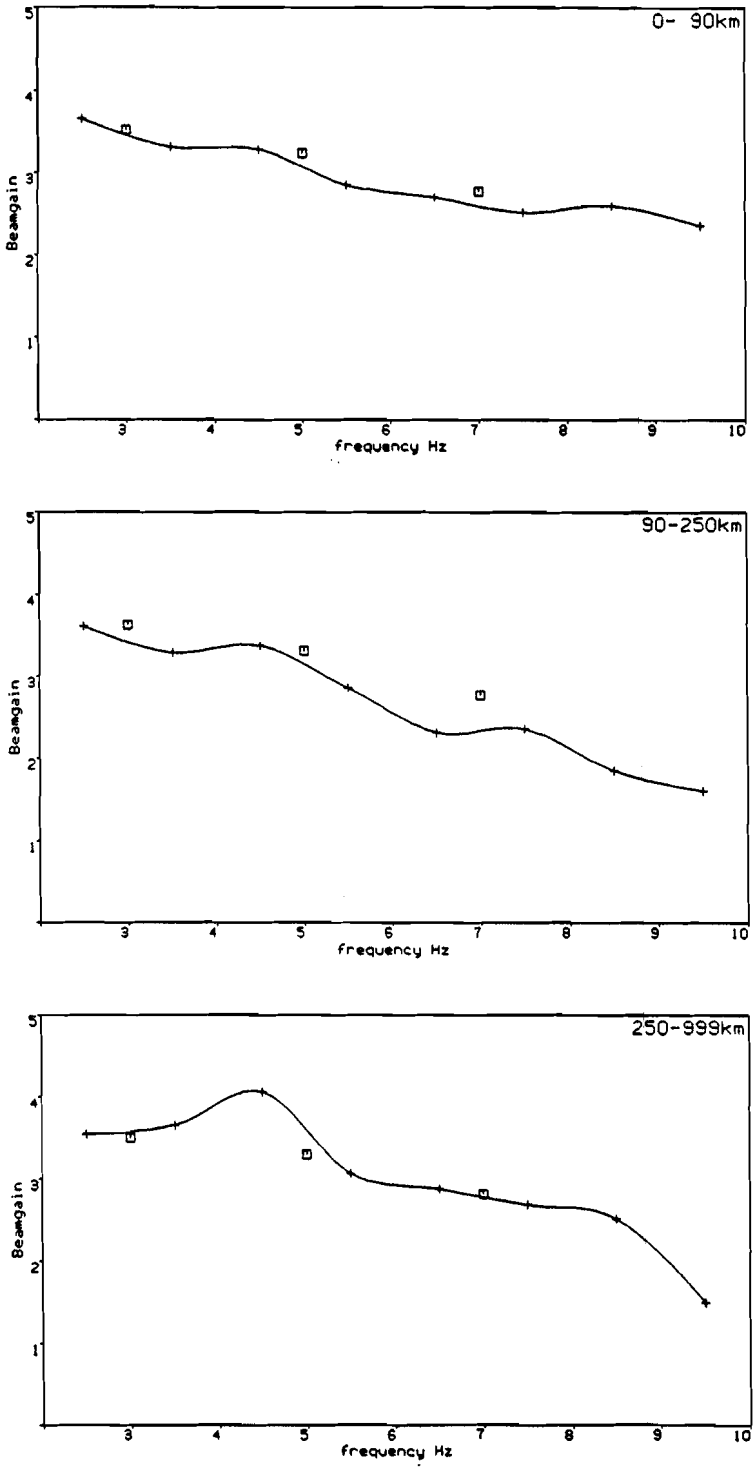

Figure 22 Signal to noise gain obtained by beamforming predicted from the observed interchannel correlations using equation 1. The predicted gains are plotted as squares. The interchannel correlations, based on 2s time windows, for the three different epicentral distance ranges and three frequency bands are computed from the exponential curves $ae^{-D/d}$ fitted to the observations given in figure 16. Also shown are the observed beam gains obtained by comparing the single channel signal and noise spectra with those for the array sum. The points represent the average for the 58 seismograms studied using a 2 sec window to compute the signal spectra.

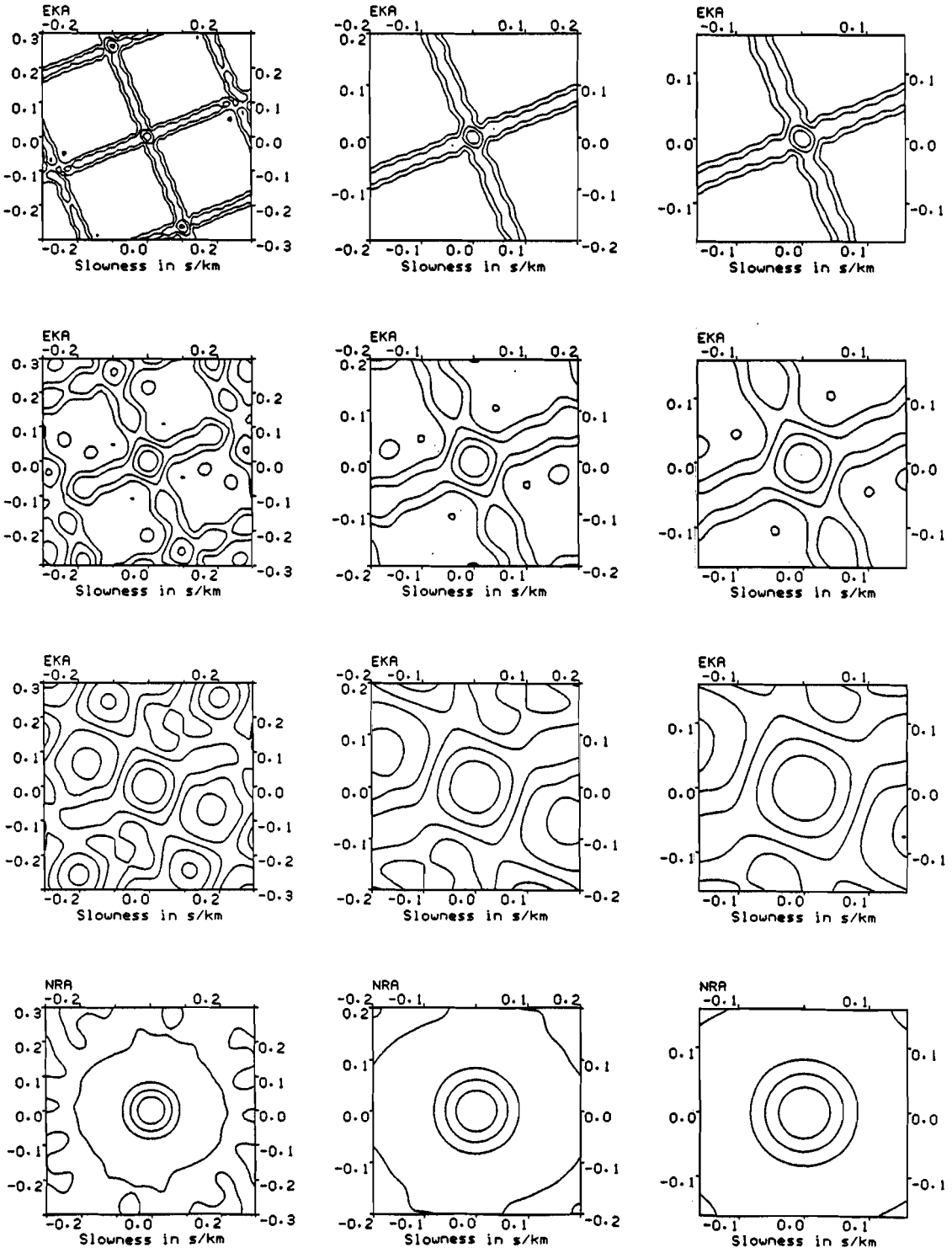

Figure 23 Array response contoured as a function of slowness for a 4Hz signal. The columns cover different slowness ranges and each row an alternative array configuration. Contours are every 0.2 in amplitude with a maximum of unity. The configurations are:
1st row: 20 channels of EKA (Full array)
2nd row: 10 channels of EKA (R1–R5,B2–B6)
3rd row: 6 channels of EKA (R1–R3,B3–B5)
4th row: NORESS array

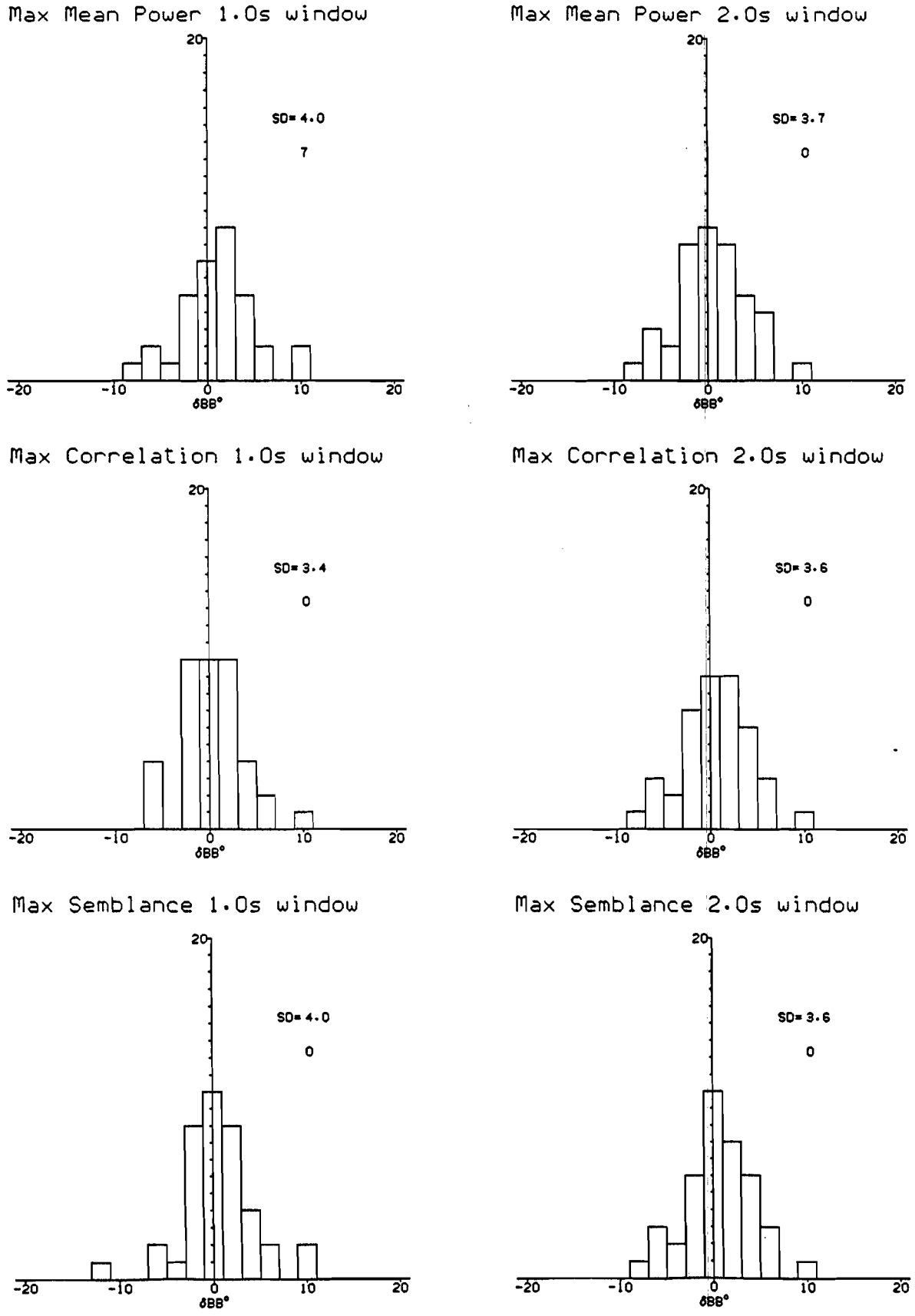

Figure 24 Histograms showing the distribution of back bearing errors δBB found using the full EKA array. The backbearings are obtained using maximum power, correlation & semblance to find the optimum beam using 1 and 2 second time windows. The values of δBB are calculated from these backbearings and those obtained from published epicentres (assumed error free). The standard deviations about zero are given on each histogram and below this the number of observations with gross errors which are not used.

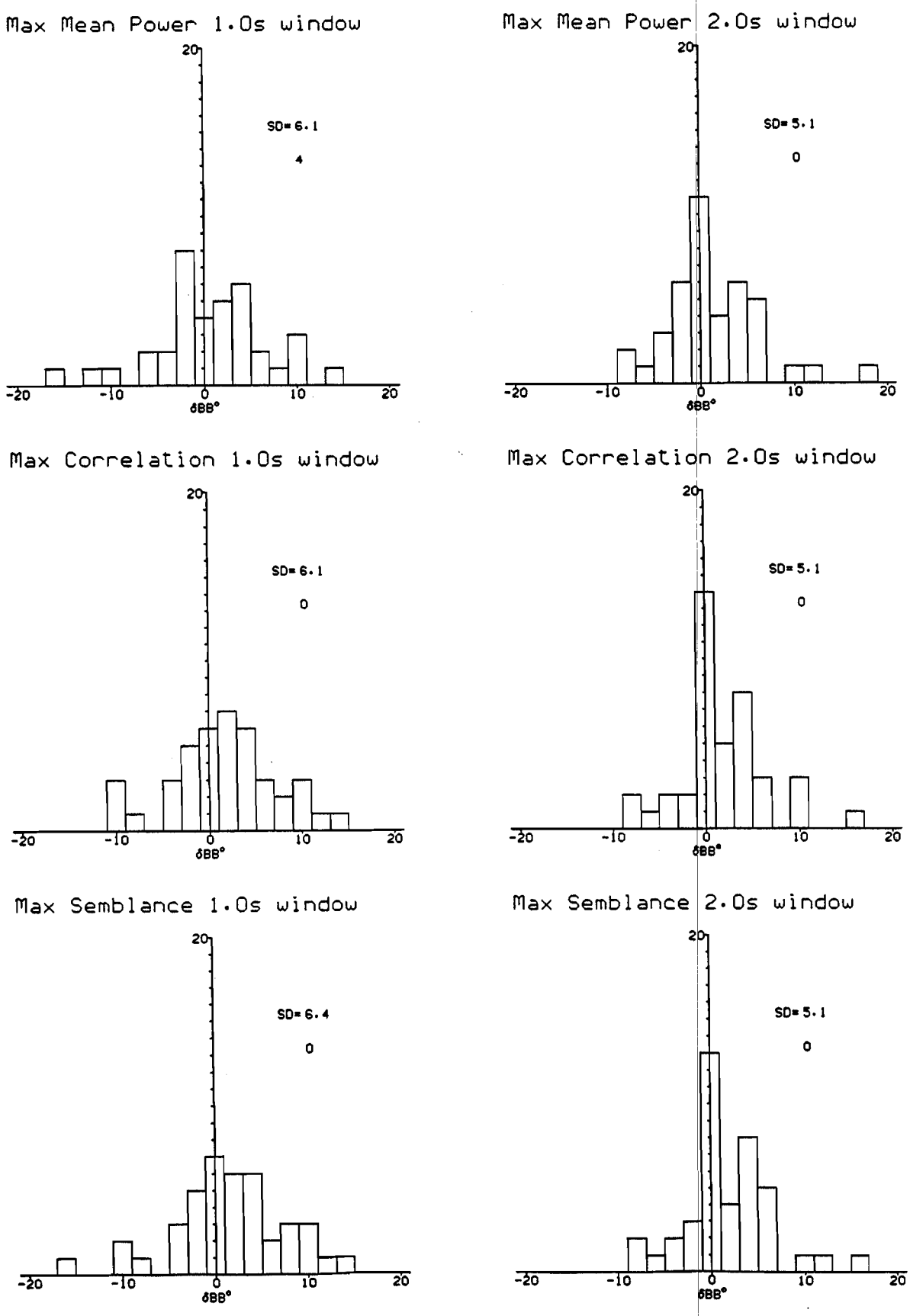

Figure 25 Histograms showing the distribution of back bearing errors δBB found using only 6 channels of EKA. The channels used are 3 from each arm which are nearest the array arm crossover operating at the time of each signal arriving. The backbearings are obtained using maximum power, correlation & semblance to find the optimum beam using 1 and 2 second time windows. The values of δBB are calculated from these backbearings and those obtained from published epicentres (assumed error free). The standard deviations about zero are given on each histogram and below this the number of observations with gross errors which are not used.

Available from
HER MAJESTY'S STATIONERY OFFICE
49 High Holborn, London W.C.1
71 Lothian Road, Edinburgh EH3 9AZ
9-12 Princess Street, Manchester M60 8AS
Southey House, Wine Street, Bristol BS1 2BQ
258 Broad Street, Birmingham B1 2HE
80 Chichester Street, Belfast BT1 4JY
or through any bookseller.

Printed in England

ISBN 0 85518196 6

UK UNLIMITED